Propulsion integration of hypersonic air-breathing vehicles utilizing a top-down design methodology

by

Brad Kenneth Kirkpatrick

A thesis submitted to the graduate faculty

in partial fulfillment of the requirements for the degree of

MASTER OF SCIENCE

Major: Aerospace Engineering

Program of Study Committee:
Thomas Gielda, Major Professor
Richard Wlezien
Thomas Ward III

Iowa State University

Ames, Iowa

2014

TABLE OF CONTENTS

LIST OF TABLES

LIST OF FIGURES

LIST OF SYMBOLS

0,1,2,3...7	Ramjet station numbering
AFR	Air to fuel ratio
α	Angle of Attack
ρ	Density
η_b	Burner efficiency
η_{th}	Thermal efficiency
η_j	Propulsive efficiency
η_{tot}	Total efficiency
g_0	Sea level gravitational acceleration
H_f	Lower heating value of fuel
M	Mach number
$\dot{m}$	Mass flow rate
P	Pressure
γ	Ratio of Specific Heats
C_p	Specific heat at constant pressure
R	Specific gas constant
I_{sp}	Specific Impulse
a	Speed of sound
T	Temperature

t	Total condition
v	Velocity
*	Sonic condition

NOMENCLATURE

CAD   Computer Aided Design

CFD   Computation Fluid Dynamics

FEA   Finite Element Analysis

GTOW   Gross Takeoff Weight

HRV   Hypersonic Research Vehicle

L/D   Lift to Drag Ratio

LHV   Lower Heating Value

MDAO   Multidisciplinary Design Analysis and Optimization

NASP   National Aero-Space Plane

OEW   Operational Empty Weight

TSFC   Thrust Specific Fuel Consumption

SERN   Single Expansion Ramp Nozzle

ACKNOWLEDGMENTS

ABSTRACT

In recent years, a focus of aerospace engineering design has been the development of advanced design methodologies and frameworks to account for increasingly complex and integrated vehicles. Techniques such as parametric modeling, global vehicle analyses, and interdisciplinary data sharing have been employed in an attempt to improve the design process.

The purpose of this study is to introduce a new approach to integrated vehicle design known as the top-down design methodology. In the top-down design methodology, the main idea is to relate design changes on the vehicle system and sub-system level to a set of over-arching performance and customer requirements. Rather than focusing on the performance of an individual system, the system is analyzed in terms of the net effect it has on the overall vehicle and other vehicle systems. This detailed level of analysis can only be accomplished through the use of high fidelity computational tools such as Computational Fluid Dynamics (CFD) or Finite Element Analysis (FEA).

The utility of the top-down design methodology is investigated through its application to the conceptual and preliminary design of a long-range hypersonic air-breathing vehicle for a hypothetical next generation hypersonic vehicle (NHRV) program. System-level design is demonstrated through the development of the nozzle section of the propulsion system. From this demonstration of the methodology, conclusions are made about the benefits, drawbacks, and cost of using the methodology.

CHAPTER 1. INTRODUCTION

The subject of hypersonic aircraft is an important one in engineering today given the recent resurgence in interest due to their potential military and space-access applications. However, hypersonic aircraft have historically had a long and complicated development process. To date, there have been few successful examples of hypersonic aircraft. Of these successful examples, air-breathing hypersonic aircraft account for only a small fraction of the total number.

1.1 Definition of Air-Breathing Hypersonic Vehicles

In the simplest terms, hypersonic flight refers to flight at high Mach numbers. However, what defines hypersonic flight and where this regime actually begins is a more complex issue. In his book, *Hypersonic and High Temperature Gas Dynamics*, Anderson describes hypersonic flow as occurring at higher Mach numbers where a number of flow effects being to come into play. These flow effects may include, among other things, high temperature gas effects, thin shock layers, and viscous interaction [1]. This also means that hypersonic flow does not correspond to an exact Mach number. However, for definitions sake, the consensus among multiple authors seems to be that this boundary is somewhere in the range of Mach 5 to Mach 7 [1, 2].

For any vehicle operating within this hypersonic regime, the two feasible propulsion options for sustained flight are either rocket motors or air-breathing jet engines. Air-

breathing jet engines, encompassing both turbine and ramjet engines, tend to be the favored option for sustained atmospheric flight. This is due to the fact that rockets need to carry both fuel and oxidizer which can result in weight and volume penalties.

At higher Mach numbers, jet engines can take advantage of ram air compression instead of using a set of compressor discs as in turbine jet engines. Engines that take advantage of ram air compression are classified as ramjets. The standard ramjet decelerates the flow to low subsonic Mach numbers so that combustion can occur. However, as the flight Mach number increases, so does the static temperature in the combustion chamber. If the static temperature is too high, flow dissociation or structural failure may occur.

Supersonic combustion ramjets, better known as scramjets, are a variation on the standard ramjet in that the flow is kept supersonic throughout the propulsion path. Since the static temperature increases as the flow is decelerated, it is advantageous to keep the air flowing through the propulsion path at a higher Mach number.

1.2 Current Design Challenges of Hypersonic Air-Breathing Aircraft

To date, there have been few flying examples of hypersonic air-breathing vehicles. Among these flying examples are the Kholod, X-43, and X-51. The X-43 and X-51 stand apart as being the only proper aircraft in this group as most of their lift was generated by aerodynamics of the vehicle.

The question is, then, what is it that makes the development of hypersonic vehicles so difficult? The difficulty may be due to a variety of reasons including technological challenges, the integrated nature of hypersonic vehicles, and project management.

Barber et al. conducted a review of available literature on hypersonic vehicles in order to identify the current limits of knowledge and technological challenges faced by the designer. The authors found that among the biggest limitations of knowledge are in propulsion and vehicle aeroshell development. Perfecting the scramjet engine is identified as a crucial issue that must be addressed. Looking further into the future, the authors also identify the need for propulsion systems and vehicle aerodynamic configurations that can operate at cruise and off-cruise conditions. Such a capability would be necessary to make hypersonic vehicles operationally viable [3].

Among the technological challenges were materials and ground testing. The focus of materials research is on materials that perform better at the high temperatures of hypersonic flight. While hypersonic wind tunnel facilities exist, the authors mention that issues such as inability to replicate flight conditions as factors that reduce their effectiveness [3].

Authors such as Bowcutt and Perrier et al. identify another major contributor to the difficulty of hypersonic vehicle design. These authors see the tendency for hypersonic vehicles to be highly integrated in nature as a source of difficulty for the designer. Bowcutt explains the integrated nature of these vehicles through a graphic of an X-43 type vehicle. This graphic demonstrates that the fuselage of this vehicle is also the primary aerodynamic lifting surface, inlet compression ramp, and nozzle of the vehicle. As one could imagine, a change in the performance of the nozzle could have a significant effect on the lift, drag, or the stability of the vehicle. In response, design tools and methods that can account for system interaction are presented as a solution [4, 5].

Finally, Tang and Chase attribute at least part of the difficulty to project management of the previous hypersonic vehicle development programs. Tang and Chase argue that certain essential elements did not exist in order for the programs to succeed in the first place. One essential element that was missing is the drive for innovation as there was no "requirements pull" or "technology push" to keep the programs moving towards the goal of an operational hypersonic vehicle. The authors also point out that these programs tended to underestimate cost and overestimate performance. When the programs failed to meet promised performance and expense targets, they would be shut down [6].

1.3   Objective

The intent of this paper is to address the integrated nature of hypersonic vehicles by changing the way that these vehicles are designed. To this end, a top-down design methodology approach is proposed for the conceptual and preliminary stages of the design process of the hypersonic air-breathing vehicle. In a top-down design methodology, a conceptual vehicle model is produced as a first step rather than being the result of an amalgamation of individually designed systems. As systems are added to the vehicle model, the vehicle is analyzed from the whole vehicle perspective and evaluated in terms of the vehicle requirements. Whole-vehicle analysis is accomplished through the use of high fidelity analysis tools such as CFD or FEA.

The purpose of the study presented in this paper is two-fold. The first objective of this paper is to discuss in detail what the top-down design methodology is and how it can be applied to the design of a hypersonic air-breathing vehicle. Chapter 2 provides some context in the form of previous design methodologies while Chapter 3 contains an in-

depth discussion about what the top-down methodology entails. The methodology is applied to a design study for a new hypersonic air-breathing research vehicle in Chapters 4 and 5.

The second objective is to critically evaluate the benefits, drawbacks, and cost involved in using the top-down design methodology. The vehicle design study presented in Chapter 6 of this paper serves as the test of this methodology. Though this design study is vastly simplified; it should be adequate to look at aspects such as analysis time or computational difficulty.

CHAPTER 2.   LITERATURE REVIEW

2.1   Engineering Design

In the simplest terms, engineering design is the way in which engineering products are conceived, developed, and delivered to the consumer. However, engineering design is much more complicated than this and the design process can involve intricate sets of procedures, analysis tools, or workflow management schemes. The purpose of this chapter is to explore the work that has already been done in this field. An introduction to the engineering design process and a set of terminology will also be presented to provide context for this literature review. However, the terminology presented in the research work can be vague and applied loosely so it is necessary to do some clarification work. An attempt will be made in this chapter to reconcile the various terminologies into clearly defined terms.

2.1.1   The engineering design process

The engineering design process has been described by multiple authors [7-9]. In his book, *Introduction to Design*, Asimow presents the design process and methodologies from a general engineering point of view [8]. Asimow describes the design process as consisting of seven sequential phases: feasibility studies, preliminary design, detailed design, planning for production, planning for distribution, planning for consumption, and planning for retirement. According to Asimow, the first three phases make up what is

called the primary design phases while the last four phases are referred to as the product life-cycle design phases. For the purposes of this study, only the primary design phases are of interest.

Raymer, along with Nicolai & Carichner have presented detailed overviews of the primary design phases as it applies to the aerospace industry in their respective design texts [7, 9]. In these two books, the primary design phases are split up into three sequential stages: conceptual design, preliminary design, and detail design. Both of these books also describe in detail what occurs in each stage of the design process.

In the first stage, conceptual design, the designer or design team starts with a design problem in the form of a set of customer requirements. The design team investigates potential solutions to these problems in the form of vehicle design concepts. Trade studies are employed to explore how various potential vehicle configurations perform. The design engineer also must be mindful of both the feasibility of the design concept and the initial customer requirements [7, 9].

The focus of the preliminary design stage is refining the design and comprehensively evaluating the performance of the aircraft. Rather than changing the overall configuration of the vehicle, refinements are made to the major assemblies, or systems, of the vehicle. In order to further evaluate the performance of the aircraft, high fidelity computational tools and real world testing are employed [7, 9].

Detail design is the last step of the design process. At this point, the design of the overall aircraft and system configuration is complete. Design of the vehicle on the

component level becomes the focus of the design team. By the end of the detail design, the aircraft design is to a point where a prototype can be manufactured and tested [7, 9].

2.1.2 Design methodology

In this section we define what design methodologies are and how they fit into engineering design. Design methodology is a term that is used frequently in literature with little to no explanation or definition of the term. However, in *A Guide to the Project Management Body of Knowledge (PMBOK® Guide)*, a methodology is described as "a system of practices, techniques, procedures, and rules used by those who work in a discipline" [10]. This definition also could be applied as a description of design methodologies. The design methodology is a set of techniques and practices that is used within the individual phases of the design process. The design process enforces what the inputs and outputs are in each phase and generally what needs to be accomplished but it does not describe how the engineer develops the product at each stage. The design methodologies are adopted by design teams based on their preferred design strategies and/or available resources. Additionally, as design teams become more interdisciplinary, methodologies may also become more intertwined to account for the interdisciplinary interaction.

2.2 Research Developments in Engineering Design

A number of different concepts have been developed in order to improve the way vehicles are designed. Among these concepts developed are parametric Computer Aided Design (CAD) modeling, integrated product development, global analysis, etc. A

selection of papers from industry and institutional research groups are analyzed to understand what design methods have been and are currently being used.

2.2.1 Integrated design methodologies and frameworks

The need to develop an integrated design methodology is a subject that is discussed often in design research papers. Integrated design refers to the ability to capture interactions between the various systems and components of a given product [4]. Bowcutt explains that the ability to identify how system and component interact allows for the exploration of potentially more cost effective, more capable, and higher performance vehicles and vehicle configurations such as scramjets or blended wing bodies [4]. A key component of integrated design is increasing the collaboration between multiple disciplines such as propulsion, aerodynamics, etc.

A number of integrated design environments have developed in recent years by industrial, governmental, and academic research groups [4, 11, 12]. One of these environments that has been discussed to great length in the literature is the Boeing Integrated Vehicle Development System (BIVDS) [4, 11]. BIVDS has been applied to the development of aircraft such as hypersonic vehicles and rotorcraft. BIVDS approach includes elements such as parameterized CAD, high fidelity analysis, and improved data management to achieve the goal of better design.

The BIVIDS approach works by developing a parameterized CAD model that by its nature can be easily manipulated to explore variations on an initial concept vehicle. These CAD models are then sent to analysis modules to evaluate the suitability of the given design. In the case of rotorcraft development, low fidelity sizing and aerodynamics

analysis modules are used [11]. However, in the case of hypersonic vehicle development, Boeing has used high fidelity tools such as inviscid CFD simulations to evaluate the performance of an aeroshell concept. Boeing uses software to drive the conceptual design process and organize the transfer of data between different vehicle analyses. In particular, Boeing uses the Phoenix Integration ModelCenter software for this task [4].

Like Boeing, Lockheed Martin has developed its own integrated design environment which is referred to as the Integrated Missile Design (IMD) environment [12]. IMD is developed for the purpose of sharing data between various disciplines. Like BIVDS, there also had been an attempt to move IMD to automated optimization. IMD uses the Adaptive Modeling Language (AML) by TechnoSoft Inc. in order to organize and drive the optimization. The difference is that AML uses built in modeling to create the vehicle model.

More recently, NASA has developed the Integrated Design and Engineering Analysis (IDEA) environment for the conceptual and preliminary design stages of hypersonic vehicles [13]. NASA IDEA is again very similar to both the Boeing BIVDS and Lockheed Martin IMD systems. IMD and IDEA both share AML as the tool for data flow management and parametric CAD modeling. The difference is that NASA's environment allows for variable fidelity analysis levels. Lowest fidelity analyses are level 0 while highest fidelity analyses are labeled as level 4. The fidelity level of the vehicles analysis increases as the vehicle design moves further through the design process.

2.2.2   Parametric CAD modeling

Parametric CAD modeling is a common element employed lately in engineering design. Parametric CAD is especially important in the integrated design environments where parameterization is necessary for design exploration.

For parametric CAD modeling, Boeing uses its own in-house program called the General Geometry Generator (GGG). GGG is used to create parameterized surface models for use in analysis software. Hirsh et al. claim several advantages of GGG over commercial CAD software. These advantages include commonality of design parameters between CAD models and design tools, smooth and consistent geometry from a parameterized model, and build vehicle design rules into the model [11].

Both Lockheed and NASA use the native CAD modeling tool in AML. AML takes an approach to modeling where a CAD model is built from a set of component "objects". Geometrical parameters of a given object are optionally tied to other objects through the model tree. Additionally, the AML system allows geometry to be imported from external CAD modeling programs without parameterization [12-14].

2.2.3   Global simulation based design

Another methodology is the use of global simulation based design. Global simulation based design refers to use of high fidelity CFD or FEA analysis of the complete vehicle. That is, systems and subsystems such as the propulsion path, wings, fuselage, and control surfaces are combined into one analysis. CFD or FEA tools are used because they are the only tools that can take into account interactions between the various systems and subsystems [15].

An earlier example of global simulation based design was developed in the mid-90s by Dassault Aviation in cooperation with the Institute of Theoretical and Applied Mechanics of the Russian Academy of Sciences [5, 15]. The methodology was developed in response to inherent difficulties in the design of hypersonic vehicles. In particular, the authors identified highly integrated vehicle geometries, minimal excess thrust, net versus individual system aerodynamic performance, and system cross-coupling as challenges in designing hypersonic vehicles [5, 15].

Due to these identified issues, the authors argue that high fidelity global vehicle analyses are needed earlier in the design process in order to accurately predict the performance of the vehicle. To this end, the authors proposed a multi-domain decomposition method for global aerodynamic computational analysis. The idea behind this method is that the analysis of a hypersonic vehicle can be split into a set of inviscid CFD simulations that are connected by a series of interfaces. These interfaces can then share information depending on how they are set up. The benefit of this method would be that the simulations could be run independently by multiple groups within an organization and each simulation could use a different fidelity level based on what is necessary for a particular component [5, 15].

High fidelity global analysis is also a feature of BIVDS. Early iterations of BIVDS used inviscid CFD simulations in order to analyze the aero-performance of the vehicle [4]. Later iterations used Reynolds Averaged Navier Stokes analysis but limited usage to the evaluation of the propulsion path [16].

One of the most recent attempts at a global analysis methodology was produced as a cooperative effort between the École Polytechnique Fédérale de Lausanne (EPFL) and

Dassault Aviation [17]. EPFL and Dassault use global CFD simulations in order to evaluate the aero-performance of a concept vehicle. The purpose of the CFD evaluation is to collect data on the performance of the vehicle and turn it into a sub-orbital flight trajectory. However, the evaluation of the vehicle was limited to the aeroshell and did not include propulsion in the simulations. Like the other Global simulation based designs, this method also used inviscid CFD simulations for aero-performance evaluation.

CHAPTER 3.   THE TOP-DOWN DESIGN METHODOLOGY

3.1   The Top-Down Design Methodology

The top-down design methodology originates from the work of Dr. Thomas Gielda. Dr. Gielda's work has been focused on the development of simulation based design tools. These tools have seen application in the DC-X program, automotive design, and consumer appliance development [18]. In recent years, a research group has been formed by Dr. Gielda to apply simulation based design to the preliminary and conceptual design of hypersonic vehicles.

The term top-down originates from the CAD modeling community and describes a type of modeling that starts by building a CAD model of an object and then dividing it into a set of component features. The original CAD model is referred to as the "parent" while the dependent features are known as the "child" features. Sets of dependencies can be built between the "parent" and "child" features to dictate how changes in the "child" feature are allowed to affect the overall model [19].

The approach of the top-down methodology is to use complete vehicle geometries as a starting point rather than building a vehicle from a set of best practice sizing rules. From these initial geometries, the systems and subsystems are gradually incorporated into the design as the design becomes more refined. The performance of these conceptual vehicles are compared with mission requirements to determine how close a given concept vehicle is to meeting the mission.

Like the integrated design methods presented in Chapter 2, parametric CAD modeling is a key component of the top-down design methodology. Referred to as the engineering concept model, the parametric CAD model is used primarily for concept exploration, weights analysis, and internal configuration. However, the CAD model can also be used for purposes such as multi-disciplinary design optimization (MDO) and as a template for construction of wind tunnel models. A representation of the usage of the engineering concept model within top-down design is located in Figure 3.1. In the context of this study, the CAD model is used solely for the purpose of concept exploration.
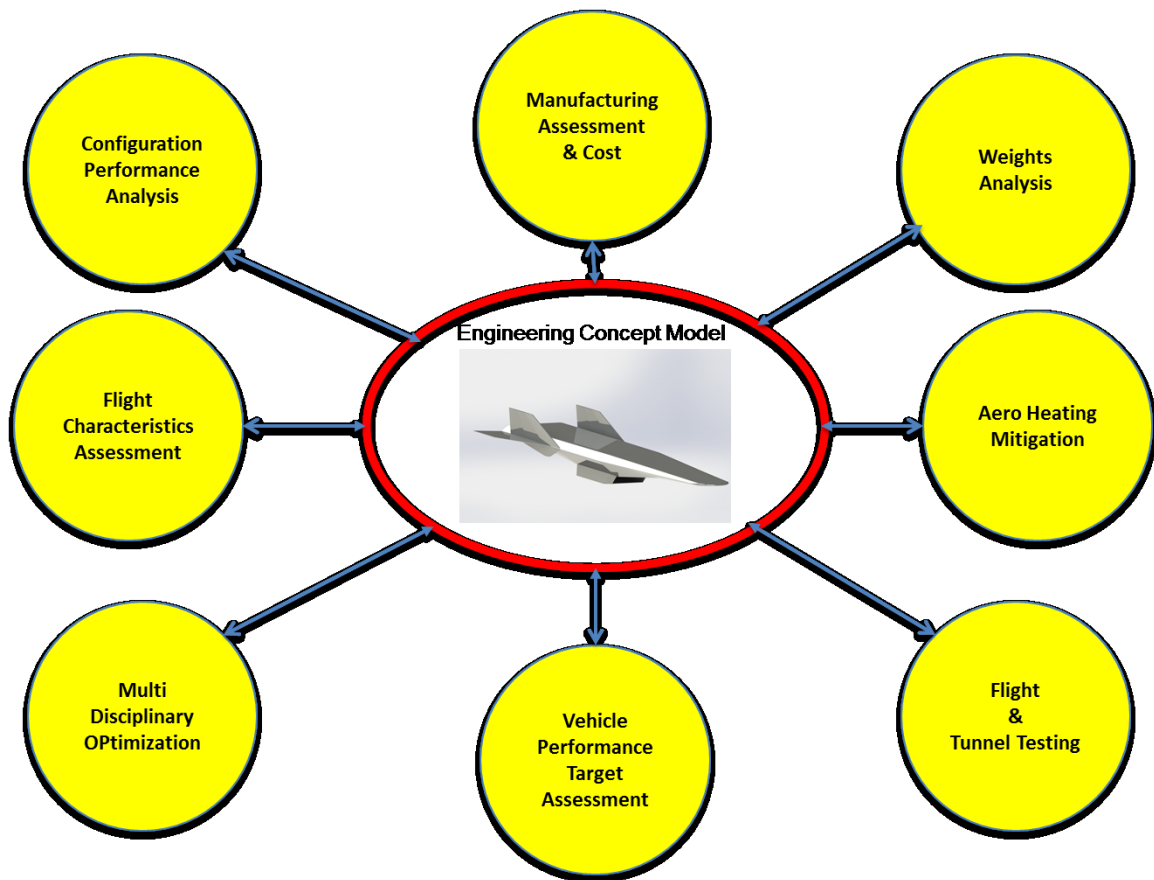
Figure 3.1 Graphic from Gielda representing the use of the parametric CAD model within the top-down methodology [20]

Rather than using purpose built or integrated CAD modelers, separate commercially available solid modeling tools are used. Solid modeling tools have a distinct advantage over surface modeling in that surface modeling can produce non-manifold geometry. By using solid models, the engineer does not need to spend extra time trying to fix a CAD model just to be able to mesh it. Solidworks has been the CAD tool of choice at Iowa State University due to its availability and built in parameterization capability. A further discussion of engineering concept models within the top-down design methodology is featured in *Parametric modeling for simulation based hypersonic vehicle design* by Alexander Lee [21].

Vehicle analysis is conducted using high fidelity analysis tools such as CFD or FEA programs. Rather than focusing on individual systems in these analyses, the emphasis is placed on complete vehicle analyses. This is a similar approach to that used by Boeing and EPFL/Dassault with their global inviscid CFD simulations. However, the top-down design methodology differentiates itself through the use of viscous CFD simulations. Viscous simulations are vital to account for flow effects such as boundary layer-shock interaction, inlet boundary layer thickness, or low speed vehicle performance.

3.2   Top-Down Design Procedure

Full understanding of the top-down methodology requires a discussion of the procedure that is used to develop a vehicle. Figure 3.2 outlines the basic design procedure of the top-down design methodology. It is important to note that this diagram may change slightly based on the vehicle being designed or the analysis elements included during the design process.

As in the traditional conceptual design stage, the design starts with customer requirements or market research which is developed into a set of mission requirements and design targets. Trade and feasibility studies are conducted in order to determine targets for each of the respective disciplines. The final step of the conceptual design stage is to analyze a
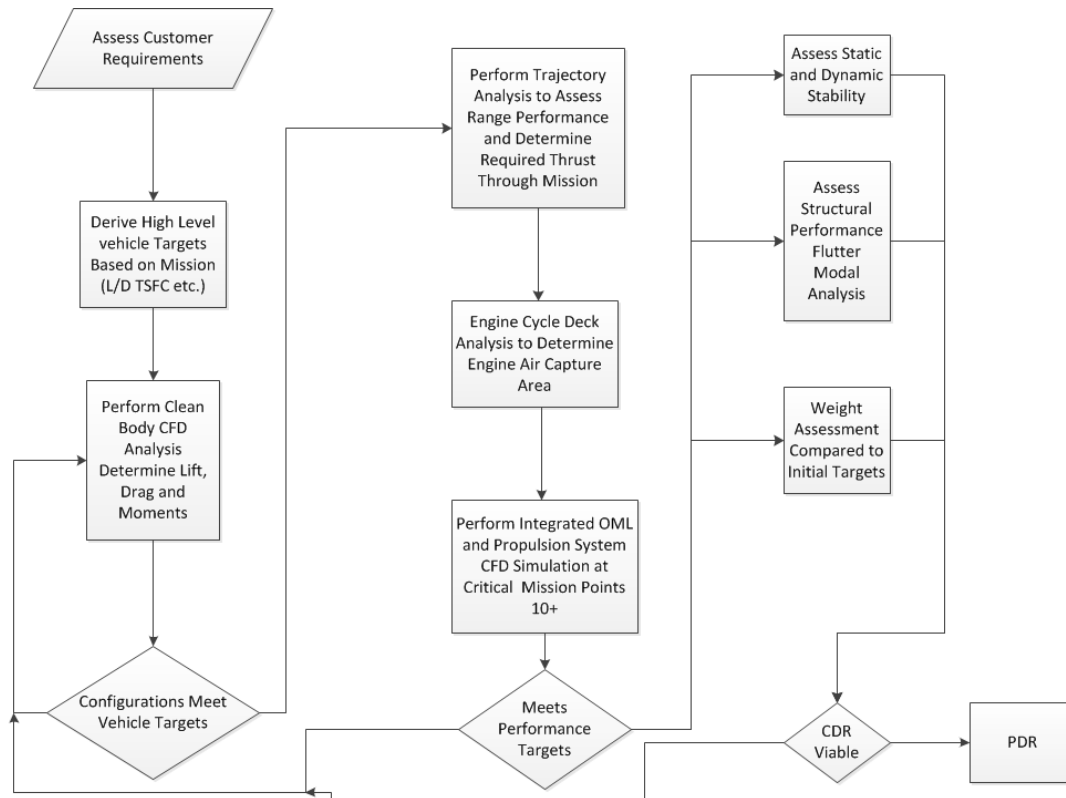
Figure 3.2: Diagram of the design procedure for the top-down methodology as presented by Gielda [20]

set of vehicle geometries from a large pool of vehicle geometries. This geometry pool is produced by the designer to explore various approaches to a vehicle design. For instance, the design team of a hypersonic vehicle might want to select a pool that includes waverider, delta wing, and blunt body configurations. Once the geometry pool is selected,

the flight characteristics of each configuration are evaluated in terms of the mission requirements. Vehicle configurations with the highest potential of meeting mission requirements are chosen for the preliminary design stage.

The focus of the preliminary design stage is the development of the systems and subsystems of the vehicle. Systems include vehicle features such as the internal structure, propulsion path, and control surfaces. System introduction and design changes are always made with the over-arching mission requirements and design targets in mind. Therefore, each system variation is rated in terms of the increased performance of the vehicle. All of the vehicle systems are incorporated into a common analysis model to evaluate installed performance of the system and ensure consistency of analysis models between disciplines. Once the design is acceptable, it can be passed on to the detail design stage or onto design optimization.

CHAPTER 4.   DESIGN PROCEDURE AND METHODS

4.1   General Analysis Procedure

The purpose of the following study is to demonstrate the top-down design methodology as applied to the development of a hypersonic vehicle. A simplified example of the design process, including both the conceptual and preliminary design stages, is used to demonstrate how vehicle systems are derived from the initial concept geometry and modified to improve its overall performance. The results of this vehicle development will be used to come to conclusions about the overall performance of the methodology and its potential application in industrial aerospace vehicle development.

The conceptual design process will be presented first. Mission requirements for a long-range hypersonic test vehicle will be defined. From these mission requirements, performance goals are developed which will be used later to evaluate the suitability of design configurations. Vehicle geometry concepts are introduced at the end of the conceptual design stage and are evaluated with CFD analyses. However in this abbreviated demonstration, only one vehicle geometry will presented to demonstrate the general process.

The preliminary design process will involve the introduction of the propulsion system and the nozzle. The nozzle concept initially will be sized using theoretical performance equations and integrated into the vehicle body. Performance of the combined aeroshell and nozzle will be evaluated using viscous CFD analyses. The results of these analyses

will be used to characterize the performance of the vehicle and the nozzle with regards to the performance goals set up in the conceptual design stage.

As subject focus was important, design and analysis was limited to integrated aeroshell and nozzle performance. Inclusion of the inlet in the study presented technical challenges that are beyond the scope of this research. Instead of simulating the entire propulsion path, a stagnation boundary condition was placed just forward of the convergent section of the nozzle. The flow conditions at this stagnation boundary were then calculated by utilizing an ideal ramjet cycle model and an equilibrium combustion calculator.

The following sections discuss the individual tools involved in the conceptual and preliminary design stages. Section 4.2 outlines the development and implementation of range analyses. The data fed into these range analyses are produced by high fidelity CFD analyses. Therefore Section 4.3 focuses on the general CFD analysis along with the associated meshing and physics models. As the inlet and combustor were not included in these simulations, an estimation of inlet and engine performance was required. Therefore, Section 4.4 describes the calculations used to estimate inlet and combustor performance. Validation was the final step to ensure that misleading results are not produced by meshing or physics modeling problems. Section 4.5 is dedicated towards validating the accuracy of the CFD analysis with an experimental benchmark case.

4.2   Range Analysis

4.2.1   Initial range estimation

Initial vehicle range calculations were performed using a Breguet range analysis. The Breguet range analysis represents a low fidelity approach to cruise range calculation. The Breguet range equation in its typical form is as follows [9]:

$$Range = -\int_{w_i}^{w_f} \frac{V(L/D)}{TSFC * W} dW = \frac{v}{TSFC} \frac{L}{D} \ln\left(\frac{W_i}{W_f}\right) \qquad 4.1$$

W_i is the initial weight at the start of the cruise segment of the trajectory while W_f is the weight at the end of the cruise segment. The velocity of the vehicle at cruise (v) is assumed. The L/D ratio and thrust specific fuel consumption are considered variables for a trade study analysis of potential vehicle ranges.

However, this method only accounts for fuel consumption at the cruise point. For other points on the trajectory, assumptions are made about the fuel consumption. These assumptions for fuel consumption are laid out in Raymer [9]. The calculation of fuel consumption for the climb portion varies based on whether the vehicle is air-dropped or not. If the vehicle departs from a runway, Raymer suggests a fuel ratio of 0.97. For the climb portion of the trajectory, an empirical calculation developed by Raymer is used. Assuming an initial Mach number of 0.1, Equation 4.2 calculates fuel consumption up to a subsonic cruise Mach number. Equation 4.3 calculates the fuel consumption up to a supersonic cruise Mach number. However, a different starting Mach number can be assumed by calculating fuel weight fraction from Mach 0.1 to the starting Mach number and then multiplying it by the fuel weight fraction of Mach 0.1 to the cruise Mach number

[9]. In the case of an air-drop, this method is used to calculate the fuel weight fraction for the entire climb phase.

$$W_i/W_{i-1} = 1.0065 - 0.0325M \qquad 4.2$$

$$W_i/W_{i-1} = 0.991 - 0.007M - 0.01M^2 \qquad 4.3$$

For Equations 4.2 and 4.3, M is the cruise Mach number, W_i is the weight of the vehicle after climb, and W_{i-1} is the weight of the vehicle before climb.

4.2.2   Optimal trajectory analysis

Utilizing the optimal trajectory analysis, as described by Nicolai and Carichner, in conjunction with complete vehicle CFD analysis, allows the engineering team to assess engineering design changes with respect to vehicle mission requirements [20]. The optimal trajectory analysis is an energy method based trajectory calculator. The concept behind energy methods is to analyze an aircraft in terms of its total energy.

$$h_e = h + \frac{v^2}{2g} \qquad 4.4$$

Specific energy (Equation 4.4) is the standard measure of the energy of the vehicle. Specific energy is the sum of the kinetic and potential energy of the vehicle divided by the vehicle weight. A key assumption made is that kinetic energy can be freely exchanged for potential energy and vice versa with no losses. Energy can be added or taken away from the vehicle by simply increasing or decreasing the speed of the vehicle

at a given altitude. This indicates that the engine is the method by which energy is added

to the vehicle.

During the 1960's, energy methods were applied by Boyd to the analysis of fighter

aircraft maneuverability [7]. Energy methods have been extended to the calculation of

minimum time and fuel consumption trajectories by authors such as Bryson et al [22].

The energy method trajectory can be used to calculate either the minimum time to

climb or minimum fuel trajectories. Equations 4.5-4.8 are the primary equations used in

the calculation of energy method trajectories.

$$P_s = \frac{dh_e}{dt} = \frac{v(T\cos\alpha - D)}{W} \tag{4.5}$$

$$f_s = \frac{dh_e}{dW_f} = \frac{dh_e/dt}{T * TSFC} \tag{4.6}$$

$$\Delta t = \int_{h_{e_1}}^{h_{e_2}} \frac{1}{P_s} dh_e \tag{4.7}$$

$$\Delta W_f = \int_{h_{e_1}}^{h_{e_2}} \frac{1}{f_s} dh_e \tag{4.8}$$

P_s is the time rate change of the specific energy of the vehicle and is referred to as excess

specific power. f_s is the rate change of specific energy per unit weight of fuel consumed

[7].

Equations 4.7 and 4.8 demonstrate that the accumulated time and fuel weight

expended are inversely proportional to P_s and f_s, respectively. Therefore, the time to

climb can be minimized by minimizing P_s at each h_e level. Equation 4.5 demonstrates

that time to climb can be minimized by maximizing available thrust (thrust minus drag) and by having a large thrust to weight ratio. Similarly, fuel consumed can be minimized by maximizing f_s.at each h_e level. f_s. can be maximized by maximizing the difference between thrust and drag or by reducing the specific fuel consumption of the engine [7].

The optimal trajectory method differs from the energy method trajectory in that the vehicle is assumed to fly at maximum L/D trajectory along the climb path. This ensures that the drag is minimum at any given point on the trajectory. However, this alone is not enough to guarantee that the point is optimal. The optimal trajectory method assumes a thrust to weight ratio for the entire trajectory. This means that at a given point on the trajectory, the vehicle will have both a weight and thrust that are independent of altitude. Therefore, the excess thrust is maximum at maximum L/D [20].

The optimal trajectory was developed as a MATLAB program. Starting weight, empty weight, thrust to weight ratio, fuel consumption data, and aerodynamic data are inputs into the program. The trajectory is calculated by iteratively reducing the weight of the vehicle from its gross weight to its empty weight. At each trajectory point the change in specific energy is calculated with Equation 4.9 [20].

$$\Delta h_e = -\frac{v}{TSFC}\left(1 - \frac{1}{\frac{T}{W}\frac{L}{D}}\right)\ln\left(\frac{W_i}{W_{i-1}}\right) \qquad 4.9$$

Given the specific energy, weight, and lift coefficient of the next trajectory point, a search is conducted to find the next trajectory point. Assuming that lift is approximately

equal to weight, the required dynamic pressure can be found by dividing the vehicle weight by the vehicle wing area and coefficient of lift. Like specific energy, the dynamic pressure is ultimately a function of altitude and airspeed velocity. As a final step, both the dynamic pressure and specific energy can be plotted on an altitude versus airspeed plot. The next trajectory point occurs where these two curves align.

4.3 CFD Analysis

All of the CFD analysis presented in this study was performed by using CD-Adapco's Star CCM+ software. All simulations used the same physics and meshing models in order to maintain consistency throughout the results. Mesh settings are an exception as different sizing settings had to be used for different models in order to generate an appropriately sized mesh. The preceding subsections detail the physics and meshing models used in the CFD simulations.

4.3.1 Physics models

All simulations were run as three-dimensional, steady state simulations. The Navier-Stokes equations were solved using the coupled flow approach. The coupled inviscid flux was generally calculated using the AUSM+ flux vector splitting scheme. The AUSM+ scheme was used as it is recommended for simulations involving high supersonic or hypersonic flow regimes [23].

As mentioned previously, simulations in the top-down design methodology model viscous effect. Turbulence was modeled using a Reynolds Averaged Navier Stokes (RANS) turbulence model. In particular, the standard k-omega turbulence model was applied. As recommended by CD-Adapco, the k-omega model is used as an alternative to

Spalart-Allmaras which has difficulty modeling boundary layers under certain conditions [23]. In addition, an all y+ wall treatment was used in each simulation.

The ideal gas model was used for the equation of state. Flow chemistry was dependent on which problem was being solved. In early simulations, the air was modeled as a single component, thermally perfect gas. For the later integrated nozzle simulations, a multi-component gas model was chosen. To reduce the complexity of the problem, a non-reacting or "frozen" chemistry model was chosen. Non-reacting chemistry would also tend to cause and underestimation of performance as recombination cannot occur [24].

Only gas components of significant quantity were chosen for representation in the model. Gas species that made up less than 1% of the total mass of the composition were neglected. The 1% limitation is significant as this is roughly the mass percentage of Argon in the atmosphere [25]. The omission these insignificant species reduced the overall amount of gas species that needed to be accounted for in the CFD simulations. The molar fractions of the remaining species then were normalized so that the total of the molar fractions added up to 1.

4.3.2   Meshing models

For each simulation, the domain was meshed by using an automatic mesh generator that is internal to the STAR CCM+ software. The majority of the domain was meshed using an unstructured polyhedral mesh. An unstructured mesh was chosen for the primary reason that it captures geometry better than a structured Cartesian mesh.

Before meshing could begin, a CAD model of the vehicle geometry is required. While STAR CCM+ has built-in CAD modeling software, an alternate external solid modeling program was chosen to build the parametric models. Solid modeling was chosen as surface models pose a significant challenge for meshing. Any gaps in the surface model will cause a non-manifold geometry error during meshing. Repairing this gap is a time consuming process and requires using the STAR CCM+ surface wrapping tool. Solid modeling does not encounter this problem so it presents a far better choice for rapid parametric design exploration.

In order to capture the boundary layer on the surface of the vehicles, a prism-layer meshing option was chosen. Many of the prism layer meshing options such as surface target and minimum sizes for the mesh were problem specific. However, the number of prism layers was held constant for all of the simulations at 15 layers. The first layer of the prism layer was sized so that a wall y+ value of between 30 and 150 is achieved [23].

Both the surface remesher and extruder meshing options were applied. According to the STAR CCM+ manual, the surface remesher is advantageous when generating prism layers as it helps in generating the outer boundary of the prism layer [23]. According to a CD-Adapco article, the extruder is used to "ensure orthogonal cells next to wall boundaries for improved turbulence and heat transfer modeling" [26].

4.4   Engine Analysis

The initial ramjet performance estimation and later calculation of pre-nozzle flow conditions used an ideal ramjet cycle analysis. The computation of the ideal cycle analysis was performed with an Engineering Equation Solver based calculator. The

ramjet cycle analysis used in this calculator is a modified version of the cycle analysis presented by Ward in his book, *Aerospace Propulsion Systems* [27].

The EES-based cycle analysis was further modified to use the 1976 U.S. Standard Atmosphere for free-stream conditions and to calculate the inlet pressure recovery past Mach 5 as provided by Mil-Spec Mil-E-5007D. The ramjet cycle analysis along with the standard atmosphere and inlet pressure recovery additions will be discussed in this section.

4.4.1 Ideal ramjet cycle analysis

For definition purposes, Ward divides the ramjet propulsion path into seven stations. Station 0 refers to the freestream conditions. Stations 1 and 2 are the ramjet inlet stations. Station 1 represents the post inlet ramp shock while station 2 represents the post shock station. Station 1 is generally not included for the ideal ramjet calculation. The flow is decelerated through the diffuser section which corresponds to station 3. The combustor of the ramjet is located between stations 4 and 5. Station 4 is the post baffle station while station 5 is the exit of the combustor. The final two stations of the ramjet are the nozzle stations. Station 6 is the throat of the nozzle while station 7 is the nozzle exit [27].
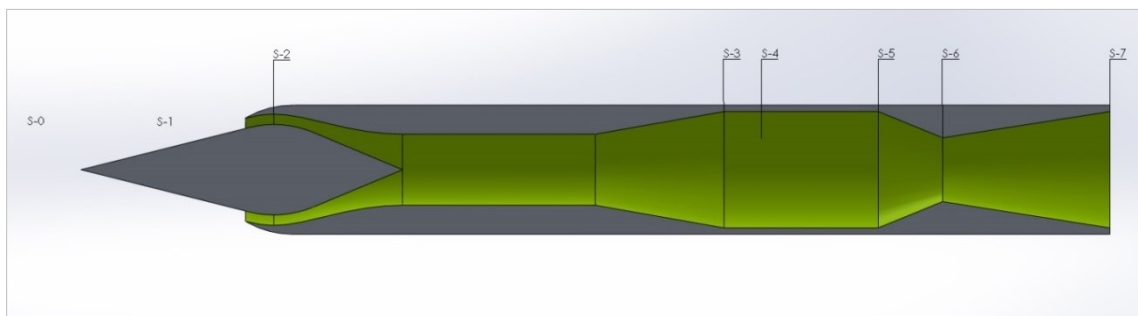
Figure 4.1: Ramjet stations as presented in Ward [27]

At each station, the static and total temperature, static and total pressure, and velocity are calculated. All of these parameters are calculated using only the calorically perfect compressible flow equations. The applicable equations are as follows:

$$P_t = P\left(1 + \frac{\gamma - 1}{2}M^2\right)^{\frac{\gamma}{\gamma-1}}$$ 4.10

$$T_t = T\left(1 + \frac{\gamma - 1}{2}M^2\right)$$ 4.11

$$a = \sqrt{\gamma RT}$$ 4.12

$$V = Ma$$ 4.13

$$P = \rho RT$$ 4.14

Equations 4.10 - 4.11 are the isentropic relations for pressure and temperature in compressible flow. These equations relate the static temperature and pressure to their respective total properties and vice versa. Equation 4.13 describes the velocity as a function of Mach number and static temperature. The ideal gas model is assumed and as a result, the density can be calculated using Equation 4.14.

It should be noted that the EES calculator varies slightly from the text in regards to the ratio of specific heats. In Ward's book, a calorically perfect assumption is made and the ratio of specific heats is assumed to be 1.4 until the post-combustion station (station 5). At the post-combustion station, a ratio of specific heats is assumed for heated combustion products. Instead, the EES calculator uses a ratio of specific heat of air that is calculated as a function of temperature and is based upon a polynomial fit of experimental data for air. The calculation of the ratio of specific heats is accomplished by

using built in functions within EES. From the post combustion stage onwards, a ratio of specific heats consistent with combustion products is assumed.

The Mach number is prescribed at each station in the engine except station 7. Behind the inlet shock at station 2, the Mach number is set to M = 0.493. The flow then is diffused before the combustion chamber and the flow reaches a Mach number of 0.1. The flow remains at Mach 0.1 through the pre-combustion and post-combustion stages which correspond to stations 3-5. Since the throat of the nozzle must be operating at a choked condition, the Mach number is specified as exactly 1 at station 6. Finally, the Mach number at station 7 is dependent on the area ratio of the nozzle. Equation 4.15 relates the nozzle area ratio and exit Mach number [28].

$$\left(\frac{A}{A^*}\right)^2 = \frac{1}{M^2}\left[\frac{2}{\gamma+1}\left(1+\frac{\gamma-1}{2}M^2\right)\right]^{(\gamma+1)/(\gamma-1)} \quad\quad 4.15$$

Total temperature is assumed constant through shocks and therefore remains constant up to the pre-combustion stage (station 4) where combustion takes place and raises the total temperature. At the post-combustion stage (station 5) onwards, the total temperature is once again held constant. The total temperature post combustion represents the combustion temperature limit of the engine.

Equations 4.16 and 4.17 are used for the calculation of the air to fuel ratio and the mass flow rates of fuel and air.

$$AFR = \frac{\eta_b H_f}{C_{p,hot}(T_{t5} - T_{t3})} - 1 \quad\quad 4.16$$

$$R_{hot} = C_{p,hot} \left(\frac{\gamma_{hot} - 1}{\gamma_{hot}} \right)$$
4.17

H_f is the lower heating value of the fuel which is dependent on which fuel is being used. η_b is the efficiency of the combustor. The ratio of specific heats after combustion, γ_{hot}, is given an assumed value of 1.25. $C_{p,hot}$ is given an assigned value of 1250 J/kgK. R_{hot} is calculated from $C_{p,hot}$ and γ_{hot} using equation 4.17.

Total pressure is assumed to be constant everywhere except for at the inlet (stations 0-2) where total pressure is estimated using Mil-E-5007D and the baffle (station 4). This is due to the assumption that the flow through the propulsion path is isentropic and that the combustion cycle is a Brayton cycle. The losses at station 4 are due to the fuel injection and combustor systems interrupting the flow. The total pressure loss at station 4 is calculated by the following equation:

$$P_{t_4} = P_{t_3} - \Phi\left(P_{t_3} - P_3\right)$$
4.18

where Φ is the baffle and mixing loss coefficient which is given a value of 2 [27]. Pressure loss occurs at stations 0-2 due to the shocks at the inlet. Mil-Spec Mil-E-5007D specifies the inlet total pressure recovery as a function of free-stream Mach number [29]. The inlet total pressure recovery standard is as follows:

$$\frac{P_{t2}}{P_{t0}} = 1.0 \quad \text{for} \quad 0 \leq M_0 \leq 1.0$$
4.19

$$\frac{P_{t2}}{P_{t0}} = 1.0 - 0.075(M_0 - 1)^{1.35} \quad \text{for} \quad 1.0 < M_0 \leq 5.0$$
4.20

$$\frac{P_{t2}}{P_{t0}} = \frac{800}{(M_0{}^4 + 935)} \quad \text{for} \quad 5.0 < M_0$$
4.21

The mass flow of the ramjet is limited by the throat of the nozzle. Therefore the ramjet size and the magnitude of the thrust of the engine are determined by the nozzle throat.

$$\dot{m} = \frac{P_t A^*}{\sqrt{T_t}} \sqrt{\frac{\gamma}{R} \left(\frac{2}{\gamma+1}\right)^{(\gamma+1)/(\gamma-1)}} \qquad 4.22$$

$$\dot{m}_5 = \dot{m}_{air} + \dot{m}_{fuel} = \dot{m}_{air}\left(1 + \frac{1}{AFR}\right) \qquad 4.23$$

Equation 4.22 is the equation for the choked mass flow rate assuming a calorically perfect flow [28]. The mass flow rate calculated by Equation 4.22 is the combination of the fuel and air mass flow rate. In order to calculate both the air and mass flow rates separately, Equation 4.23 is used to first calculate the mass flow rate of air and then it is simple matter of subtraction to find the mass flow rate of fuel. Once all of the flow parameters have been solved for, the thrust can be calculated using Equation 4.24.

$$T = \dot{m}_e v_7 - \dot{m}_i v_0 + A_{exit}(P_7 - P_0) \qquad 4.24$$

4.4.2   Standard atmosphere

For a specified flight Mach number and altitude, the 1976 U.S. Standard Atmosphere was used to calculate freestream static and total pressure, static and total temperature, density, and air-speed. For geopotential altitudes lower than 85 km, a calorically perfect gas model and constant composition gas are assumed [25].

As a result of these assumptions, both the ideal gas equation (Equation 4.14) and the speed of sound equation for a calorically perfect gas (Equation 4.12) are applicable. Equation 4.13 relates the flow velocity to the Mach number and the speed of sound. Additionally, the air can be considered to have a constant composition from sea-level to 85 km. As such, a ratio of specific heats of 1.4, a mean molecular weight of 28.9644 kg/kmol, and a specific gas constant of 287.0531 J/kgK are assumed constant over this range of altitudes [25].

Air-speed and density now become a function of Mach number, static pressure, and static temperature. The 1976 Standard Atmosphere provides a set of equations to describe static temperature and pressure as a function of geopotential altitude. The equations for the standard atmosphere below 86 km are as follows:

$$T = T_{M,b} + L_{M,b} \cdot (H - H_b)$$
4.25

$$P = P_b \cdot \left[\frac{T_{M,b}}{T_{M,b} + L_{M,b} \cdot (H - H_b)} \right]^{\left[\frac{g_0' * M_0}{R^* \cdot L_{M,b}} \right]}$$
4.26

$$P = P_b \cdot exp\left[\frac{-g_0' \cdot M_0(H - H_b)}{R^* \cdot T_{M,b}} \right]$$
4.27

Equation 4.25 describes the static temperature as a function of geopotential altitude. $L_{M,b}$ is defined as the molecular scale temperature gradient and has units of K/km. Up to 84 km, there are 7 regions each with differing values for the molecular scale temperature gradient. A region with an $L_{M,b}$ of zero is an isothermal region whereas a non-zero $L_{M,b}$ represents a gradient region. $T_{M,b}$ is the temperature at the base of each of the gradient

regions. H is the geopotential altitude while H_b is the reference altitude for each of these gradient regions [25].

Equation 4.26 describes the static pressure as a function of geopotential altitude for gradient regions. Equation 4.27 describes the static pressure as a function of geopotential altitude for the isothermal regions. M_0 is the sea-level molecular weight which is essentially constant up to 86 km. P_b is the pressure at the base of the atmospheric region. g'_0 is a dimensional constant that relates the geopotential meter to the standard meter [25]. Total pressure and total temperature are calculated from static pressure and temperature using equations 4.10 and 4.11, respectively.

4.4.3   Combustion and nozzle chemistry analysis

A key component of the high-fidelity CFD simulations was the inclusion of combustion chemistry. Heated air and heated combustion products have a completely different ratio of specific heats which can ultimately change the results of the nozzle analysis.

Ramjet combustion was modeled by adding combustion product species to the propulsion path via a stagnation boundary condition. The calculation of the combustion product was performed by using an equilibrium chemistry calculator using the post combustion chamber station (station 5) flow conditions. In this study, the NASA Chemical Equilibrium with Applications (CEA) calculator was chosen for equilibrium calculations [30].

Constant pressure and assigned enthalpy constraints were placed on the analysis. The constant pressure condition is due to the assumption of a Brayton cycle for a ramjet

engine. The key assumption of the Brayton cycle is that combustion occurs at constant pressure [31]. Additionally, the assigned enthalpy constraint means that adiabatic flame temperature is being calculated. Heat transfer and mechanical work is assumed negligible for assigned enthalpy [31].

The composition of the combustion products was obtained by first obtaining the air to fuel ratio from the ideal ramjet cycle analysis. Air and fuel were added in quantities consistent with this air to fuel ratio. To reduce the complexity of the problem for CFD analysis, only significant species were analyzed. This means that species like Argon, which makes up roughly 1% of air by mass, were neglected [25]. As a result, inlet air was assumed to be 77% Nitrogen and 23% Oxygen by mass. Flow parameters such as initial static temperature and static pressure were input into the program. Final static temperature and composition of combustion products were output from the program. Species that made up less than 1% of the combustion products by mass were neglected.

Flow exiting the combustor was assumed to be non-reacting. That is, the flow composition as calculated in the combustor via the CEA calculator is held constant throughout the nozzle. This decision was made for two reasons. First, non-reacting flow represents a conservative calculation of the nozzle performance as recombination cannot occur if the flow has begun to dissociate [24]. Second, the addition of reacting flow would have increased the complexity of the problem. This would have made it difficult to obtain a solution within the timeframe of the study.

4.5   Validation of Computational Tools

To prove the usefulness and accuracy of the methods presented in this study, it was necessary to validate the physics models and meshing methods used in the CFD analysis.

4.5.1   Validation case description

Validation was performed by reproducing the experiment data presented in NASA Technical Memorandum 4638 "Experimental Results for a Hypersonic Nozzle/Afterbody Flow Field" by Spaid, Keener, and Hui [32]. TM-4638 was an experimental study conducted in the mid-90s in response to the need for validation of CFD codes used in the NASP program.

The study involved testing a vastly simplified representation of an after-body with a single expansion ramp nozzle (SERN) in the NASA Ames 3.5-foot Hypersonic Wind Tunnel. The scramjet model was developed for freestream Mach numbers of 5.3, 7.3, and 10 but was tested experimentally at approximately Mach 7.33 [32, 33]. Rather than expelling combustion products through the nozzle, air was fed into a stagnation chamber and then expelled through the nozzle.

The experiment collected data on the following flow characteristics: total pressure, total temperature, static pressure, static temperature, skin friction, boundary layer profiles, boundary layer displacement, momentum thickness, and flow direction. Most of the data collection was focused on evaluating flow at the ramp, nozzle, and nozzle plume. Thus, a majority of the surface probes are concentrated on the ramp and the nozzle of the body. A two degree of freedom probe was also used to measure flow at various

increments within the plume [32]. A full detailed account of station locations and experiemntal equipment is available on pages 3 and 4 of the report [32].

4.5.2 Validation simulation setup

Included in the appendices of TM-4638 were a full set of plotted data from the experimental testing of the after-body model. The objective of the validation case was to reproduce data from a few select plots representative of the general flow characteristics. The validation case was setup using the same CFD and CAD modeling tools as used in the vehicle study presented in Chapter 5.

The first step in setting up the validation case study was to reproduce the after-body geometry. The geometry of the model was created using SolidWorks. Basic geometry was replicated including the boundary layer rakes, the aeroshell, and the nozzle. Geometrical features such as the stand and the flow probes were not reproduced due to the additional computational complexity of including these components. Additionally, exact dimensions of these features were not included in TM-4638. Attempting to include these features would
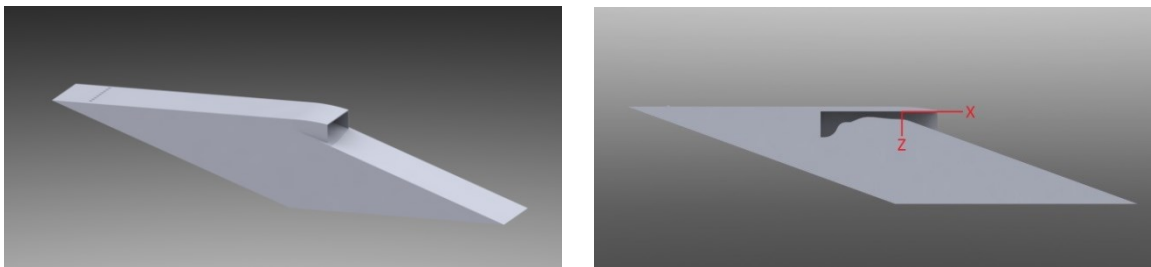

Figure 4.2: CAD representation of the afterbody model from NASA TM-4638

have significantly complicated the modeling process. Once the modeling was finished, the CAD file was then exported to the CFD analysis software, STAR CCM+, as a parasolid file.

The next step in the validation case study was to set up to the computational model in STAR CCM+. Once the parasolid file had been imported into STAR CCM+, the computational domain could be set up. For a wind tunnel validation simulation, the outer walls of the computational domain would normally be identical in shape and dimension to the walls of the actual wind tunnel. The purpose of replicating the wind tunnel walls is to mimic the blockage effects caused by the wind tunnel walls which results in skewed flow measurements.

However, there was no available information on the size or geometry of the testing section of the NASA Ames 3.5 ft. Hypersonic wind tunnel. As a result, an assumption was made that the blockage effects would be minimal and so no attempt to model the wind tunnel models was made. Instead, a square domain was built around the afterbody and appropriately sized in order to allow the proper propagation of shocks and the jet plume. The CD Adapco recommended domain sizing for simulations of this type is a domain eight times the size of the analyzed model in each dimension [23].

The boundary conditions of the outer domain surfaces (shown in Figure 4.4) were chosen in order to mimic the NASA experiment as closely as possible. The inlet to the domain was set up as a freestream boundary condition which allowed Mach number, static pressure, and static temperature to be specified. The outlet of the domain was set as a pressure outlet with the static pressure set to match that of the freestream static pressure. On the remaining three

Figure 4.3: Computational domain of the afterbody validation case

tunnel wall surfaces, a pressure outlet boundary condition was used rather than a wall boundary condition. Additionally, the problem was symmetric and as such, the problem was divided along the centerline and a symmetry boundary condition was applied to the newly created surface.

The surfaces of the scramjet after-body model, including the outer mold line and the nozzle, were given a no-slip wall boundary condition. In the original NASA experiment, the flow through the nozzle was generated by pumping air into high pressure reservoir or plenum. Rather than modeling the entire plenum and feed system in the simulation, a stagnation boundary condition was used where total pressure and total temperature were specified.

The validation simulation employed the same meshing and physics models as the generic vehicle analysis which were presented in section 4.3 This ensured that conclusions drawn about the accuracy of the validation case could also be applied to the CFD analysis stage of the top-down design methodology in general. For this validation simulation, however, there were a few unique settings.
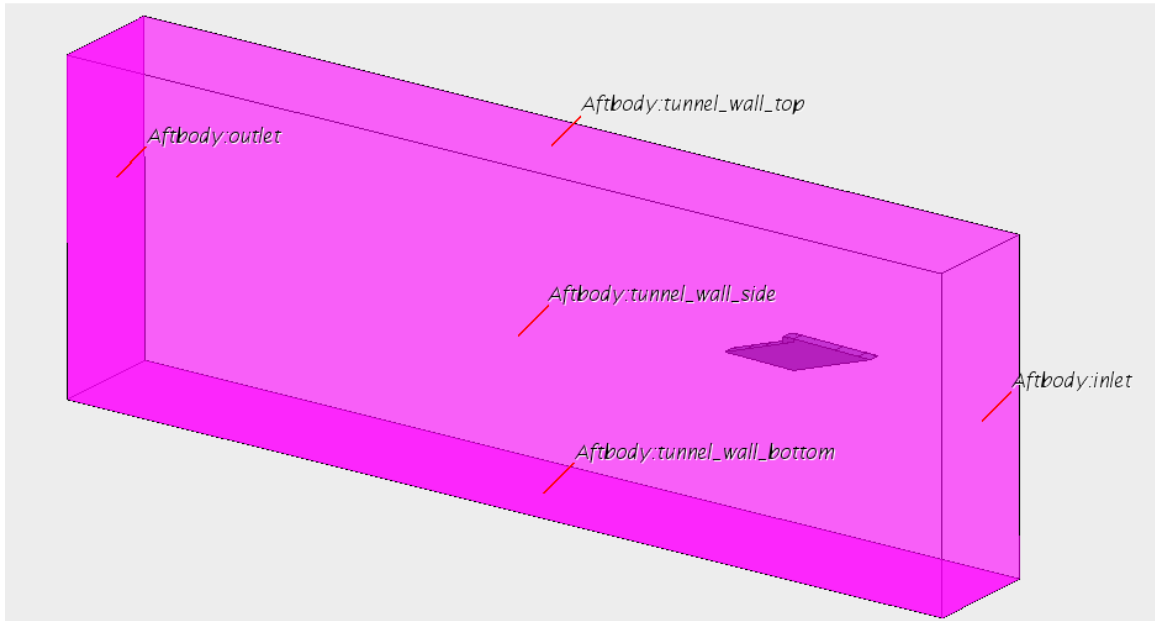
Figure 4.4: Boundary surfaces on the outer computational domain

In the meshing stage, the polyhedral mesher with the prism layer meshing applied. The prism layer was given 15 layers, a stretching of 1.1-1.25, and a thickness of 0.375 cm to 1.875 cm. For the polyhedral mesh, surface size on the after-body surfaces were minimum size 0.01 to 0.5 cm while the target size ranged from 0.05 to 0.1 cm. On the outer domain, the surface size was a lot larger with a minimum size of 0.25 m and a target size of 0.5 m. Meshing of the domain resulted in a total cell count of 944,814 cells.

The physics settings used were the same as detailed in subsection 4.3.1. The only exception was the courant number which was given a value of 2. The simulation was run as a parallel processing simulation and was allotted 5 processes. When the simulation was run with parallel processing, the total computation time of the simulation was approximately 16.5 hours.

4.5.3   Results analysis and comparison with experimental data

For comparison purposes, a number of plots from TM-4638 were chosen. The first of these plots were the ratio of static pressure to jet total pressure (p/p_{tj}) on the surface of the ramp which are displayed in Figures 4.5-4.8. p/p_{tj} was measured at a series of taps 0, 2.880, 6.878, and 7.991 cm from the centerline along the y-axis.

A comparison of the experimental and CFD validation case ramp p/p_{tj} show a close agreement between the two sets of results. The only discrepancy in the results shows up at approximately x = 5 cm. The CFD results show a lower pressure ratio than is recorded in the experiment. This corresponds to a section of the ramp that is roughly midway between the origin and the cowl trailing edge.

Boundary layer data also was chosen for comparison in order to determine the accuracy of the boundary layer calculation. A comparison of the computational and experimental profiles at the aft boundary layer rake (x = 0.49 m) is presented in Figure 4.9. This comparison shows a significant difference between the two results which increases with distance from the ramp surface. This seems to indicate either that the CFD calculated boundary layer is thicker than in the experiment or that there is a higher positive pressure gradient in the experiment. However, the second option could be discounted since the experimental and computational ramp pressure profiles match up exactly at the aft boundary layer rake.

Figures 4.10 and 4.11 plot the flow angle and impact pressure, respectively, for the x = 10.29 cm. station. Figure 4.10 indicates close agreement between experimental and CFD results with the exception of two deviations. The first deviation is in the vicinity of

z = 0 cm. where the CFD results show a sudden jump in the flow direction to roughly -32.5 deg. This deviation seems to be due to a lack of data in the experimental results at this point. The second deviation occurs roughly between z = -2 cm. and z = -4 cm. which is just above the trailing edge of the cowl.

Figure 4.11 deviates significantly from the experimental results, especially in the freestream region above the cowl at z = -4 cm. to z = -15 cm. The difference between the pressure measurements may be due to the freestream conditions. At freestream conditions, the total pressure is 6,895 kPa and the total temperature is 828 K. Assuming the isentropic gas relations hold, the static pressure would be 1206 Pa while the static temperature would be 70 K. At 77 K, Nitrogen condenses into a liquid [34]. However, this condensation behavior is absent from the CFD simulation. This seems to indicate that the homogenous ideal gas assumption may be flawed for the given combination of total temperature, total pressure, and Mach number in this experiment. This would in turn affect the calculation of P_{t2} as the calculation relies on the calorically perfect isentropic flow and normal shock equations.
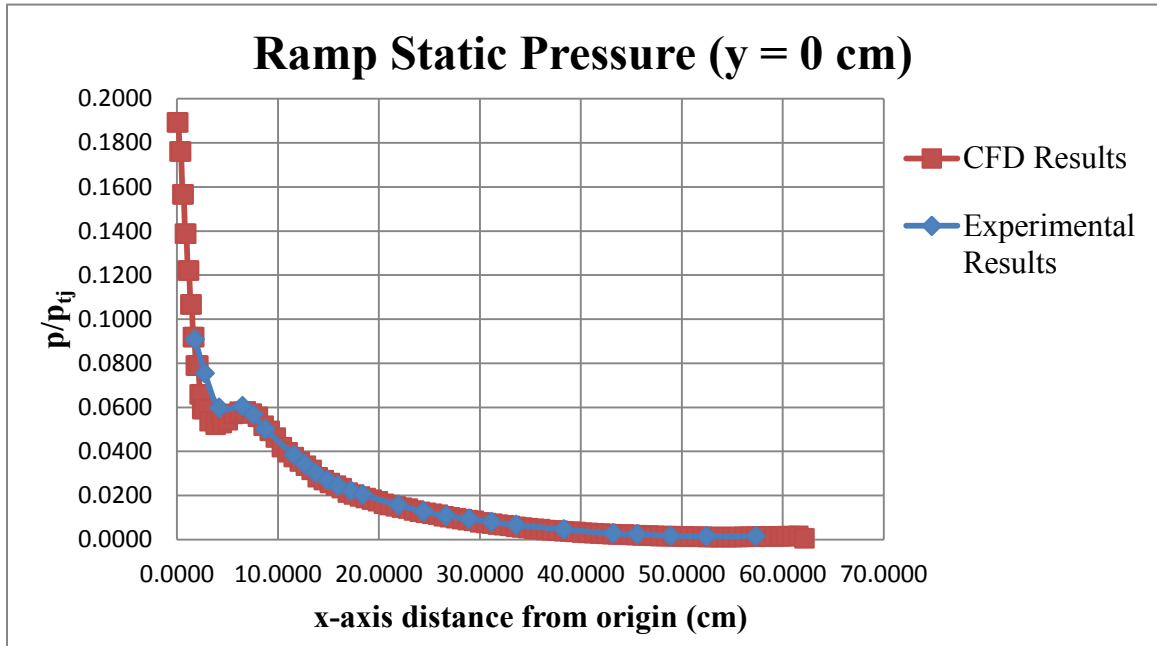
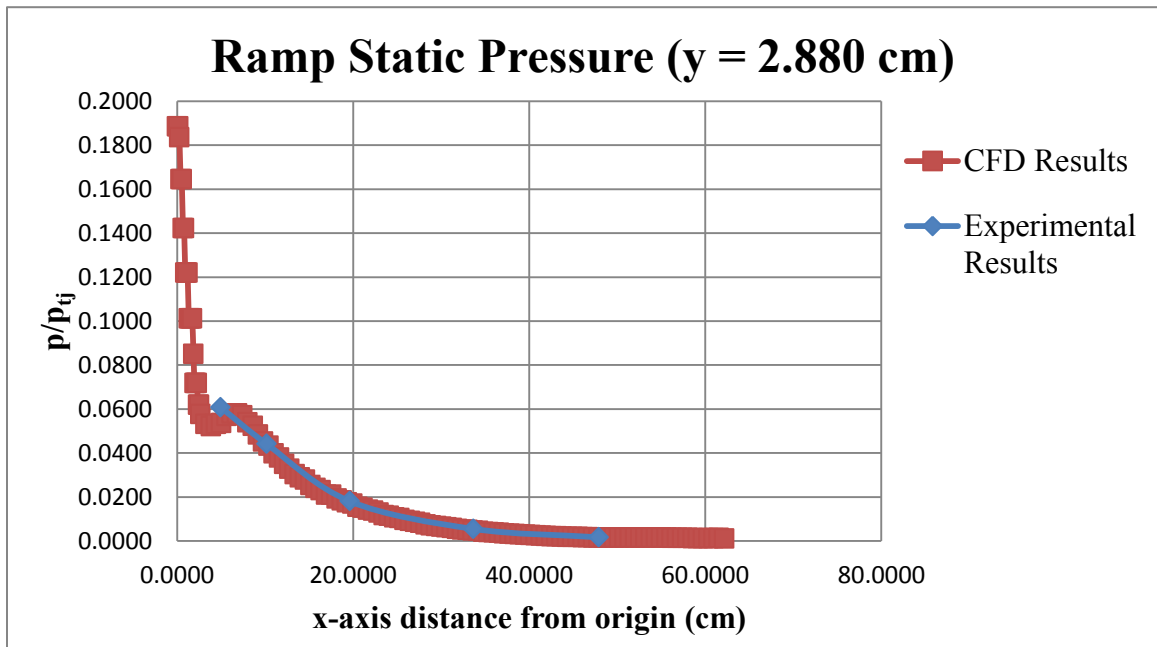Figure 4.5: p/ptj vs x-axis distance from origin (y = 0 cm)

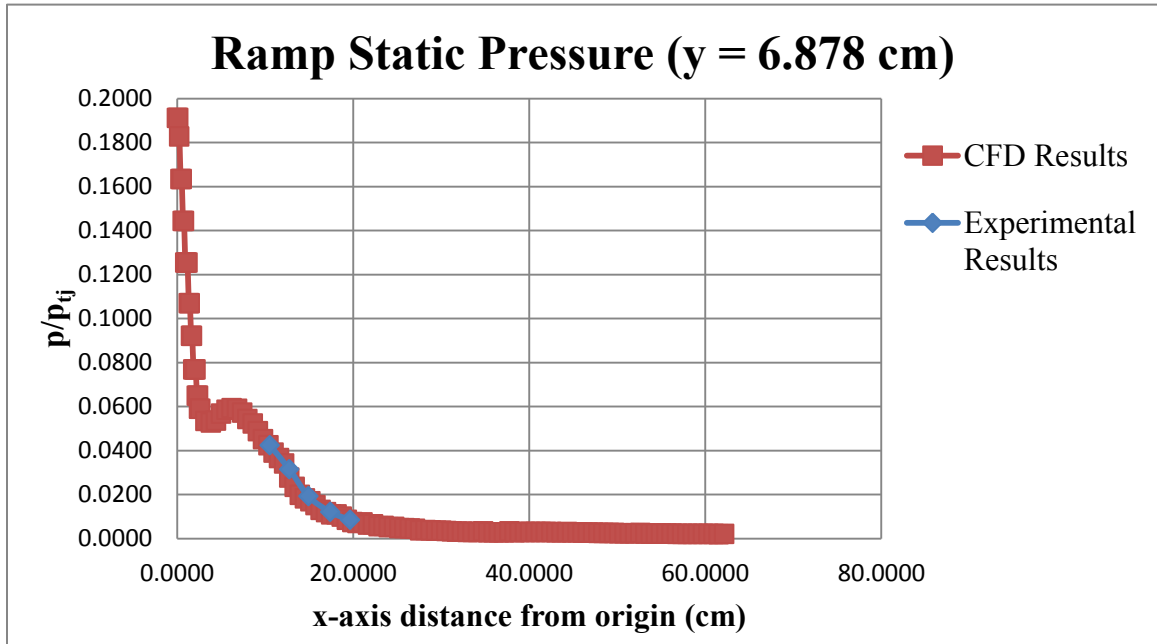Figure 4.6: p/ptj vs x-axis distance from the origin (y = 2.880 cm)

Figure 4.7: p/ptj vs x-axis distance from the origin (y = 6.878 cm)
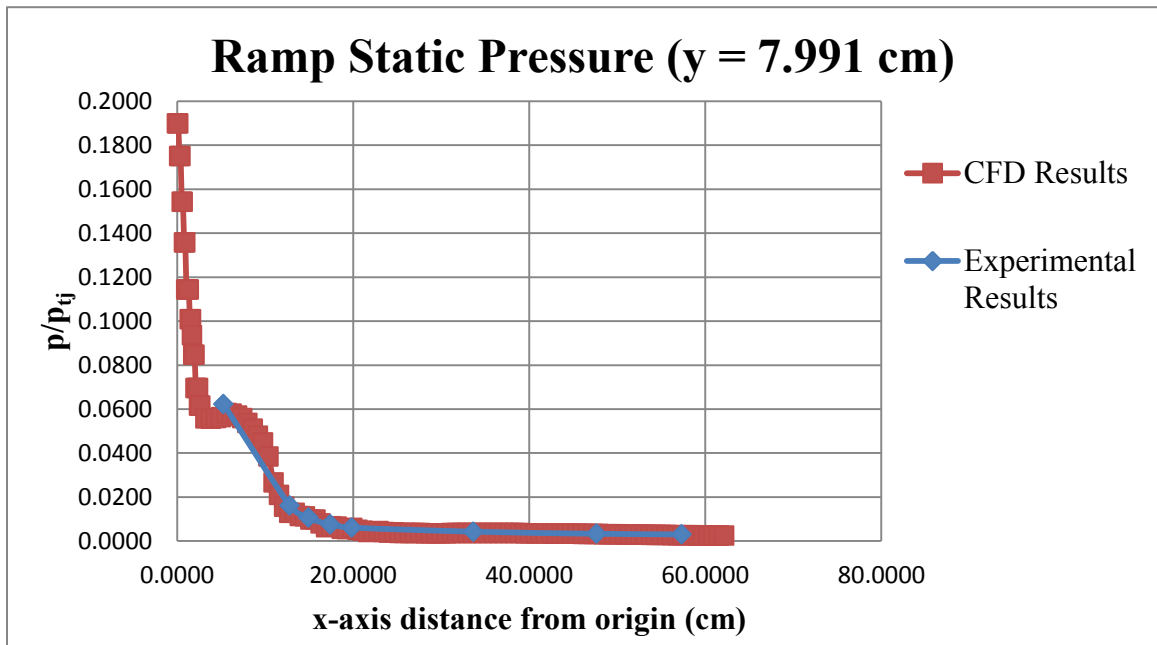
Figure 4.8: p/ptj vs x-axis distance from the origin (y = 7.991 cm)

Figure 4.9: Ramp Boundary Layer Profile – Aft Rake, $p_{tj}/p_\infty = 312$

Figure 4.10: Flow-angle, x = 10.29 cm

Figure 4.11: Impact Pressure, x = 10.29 cm

Figure 4.12: Absolute pressure plot from the computational validation case

Figure 4.13: Mach number plot from the computational validation case

Figure 4.14: Oil-streak on ramp of the computational validation case

.

CHAPTER 5.   DESIGN OF A GENERIC HYPERSONIC AIR-BREATHING VEHICLE
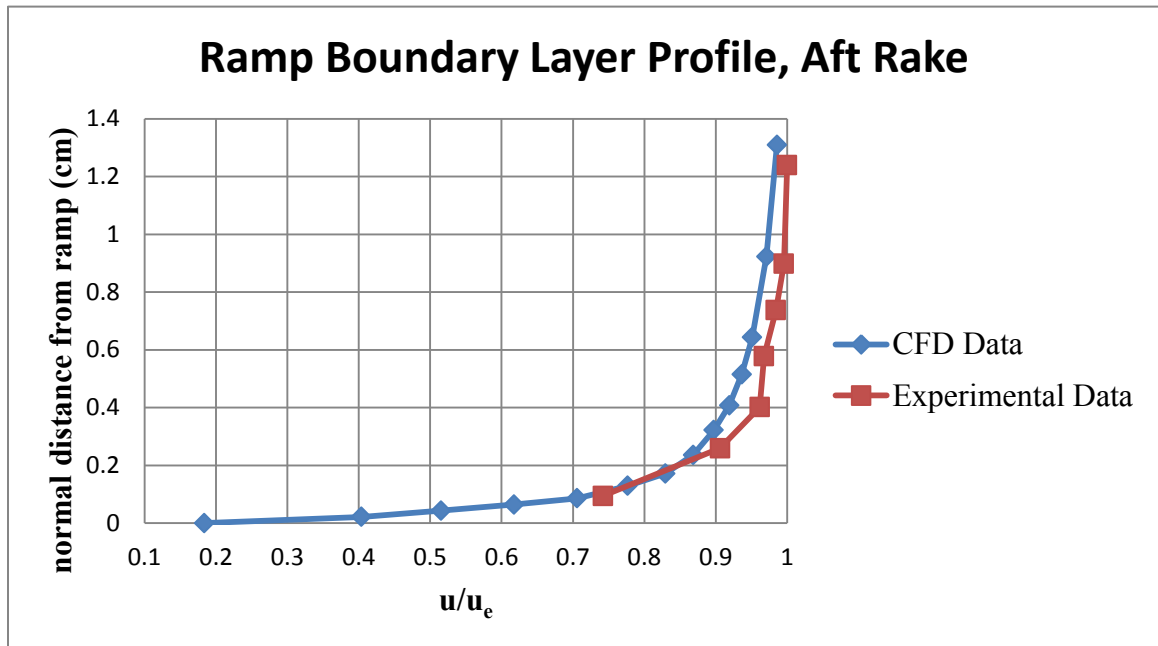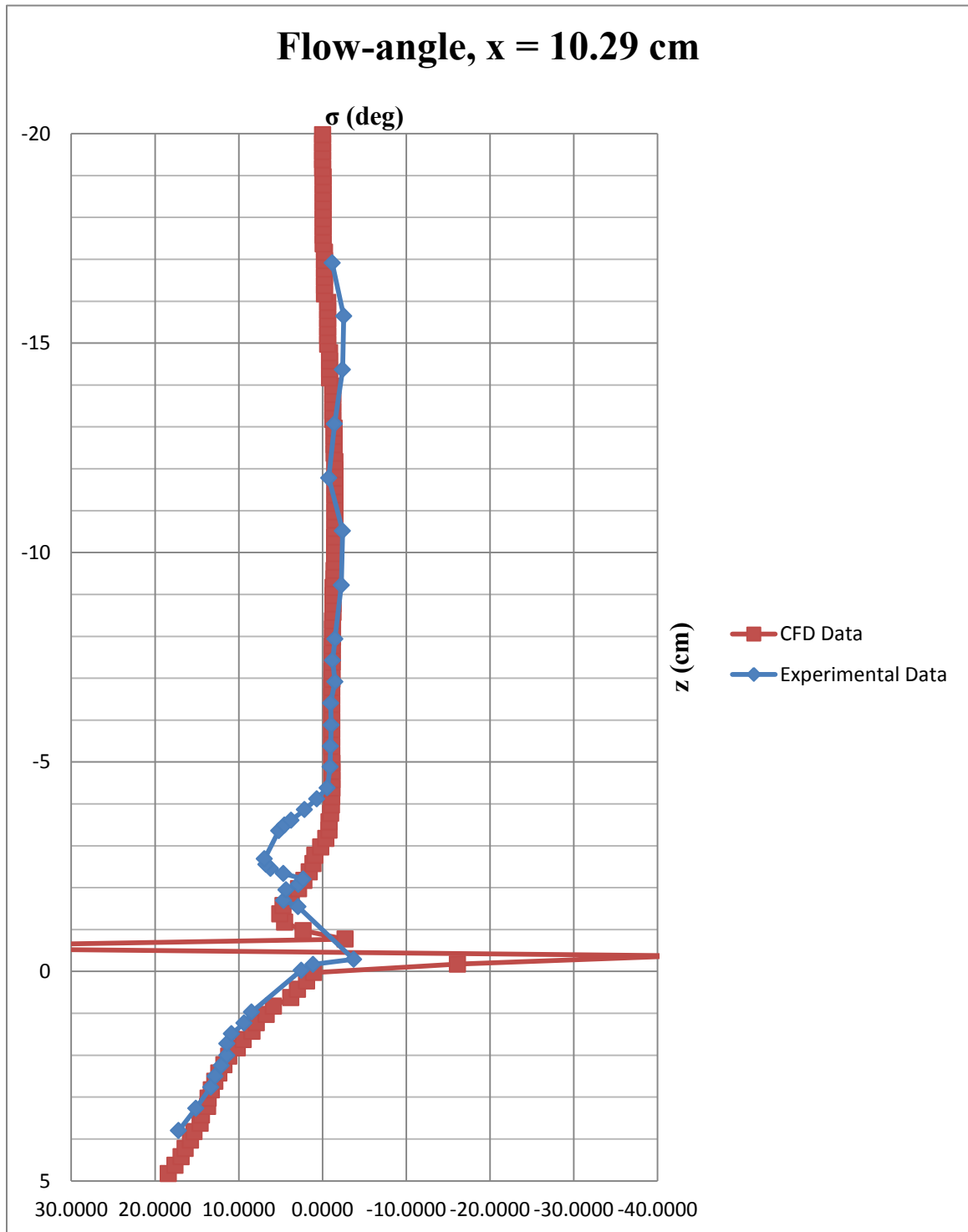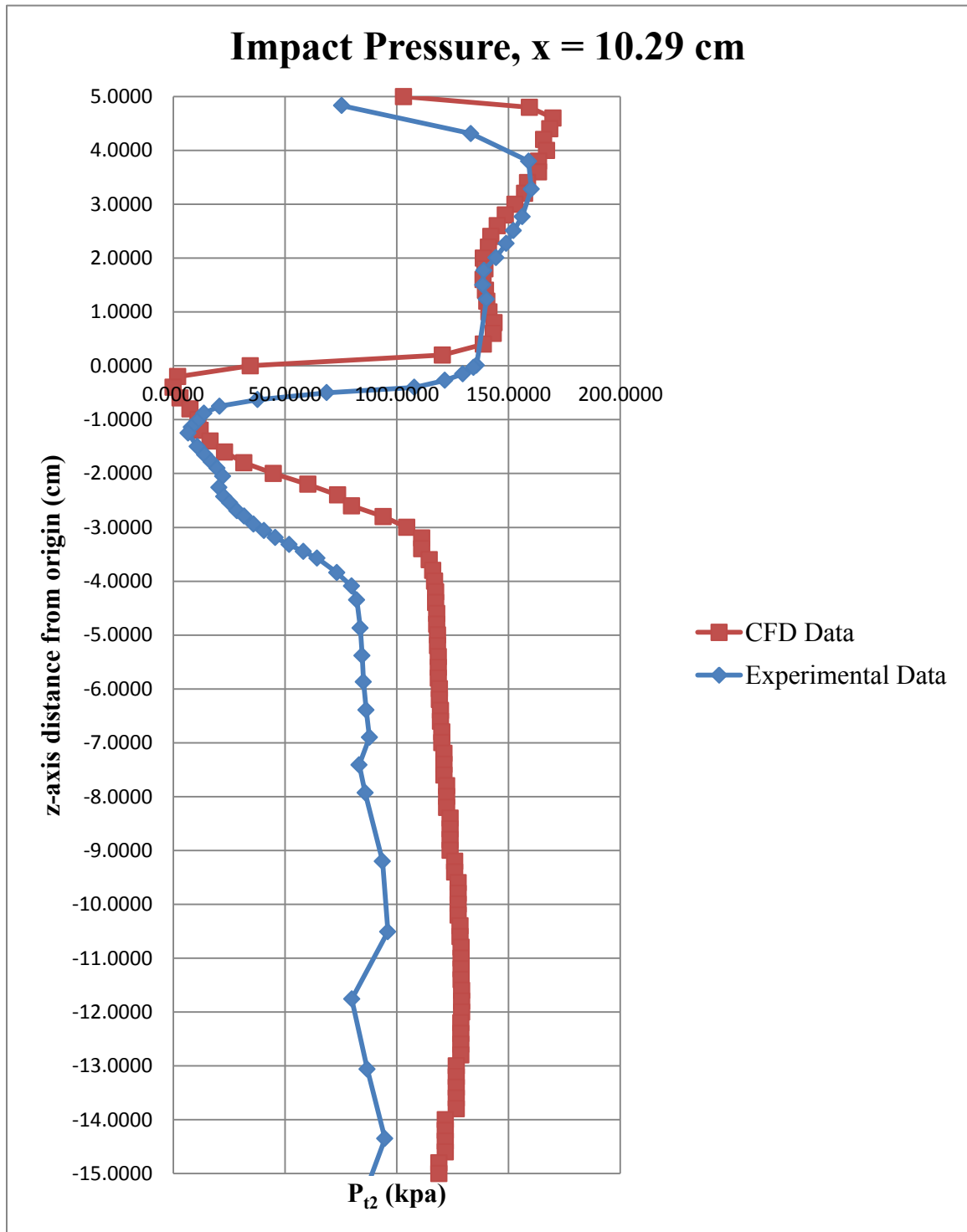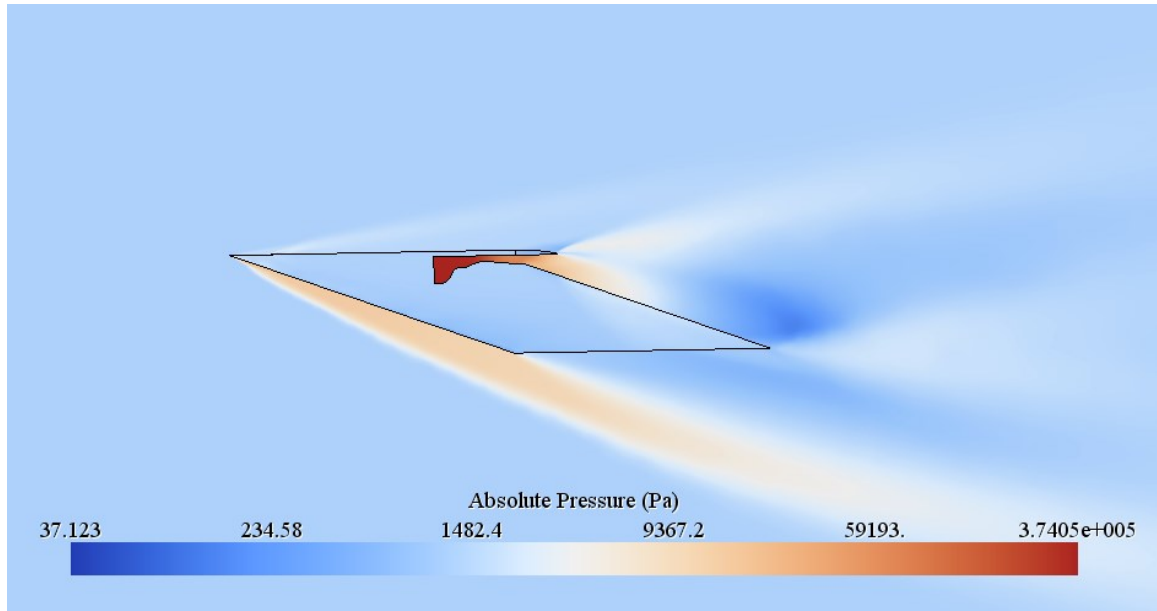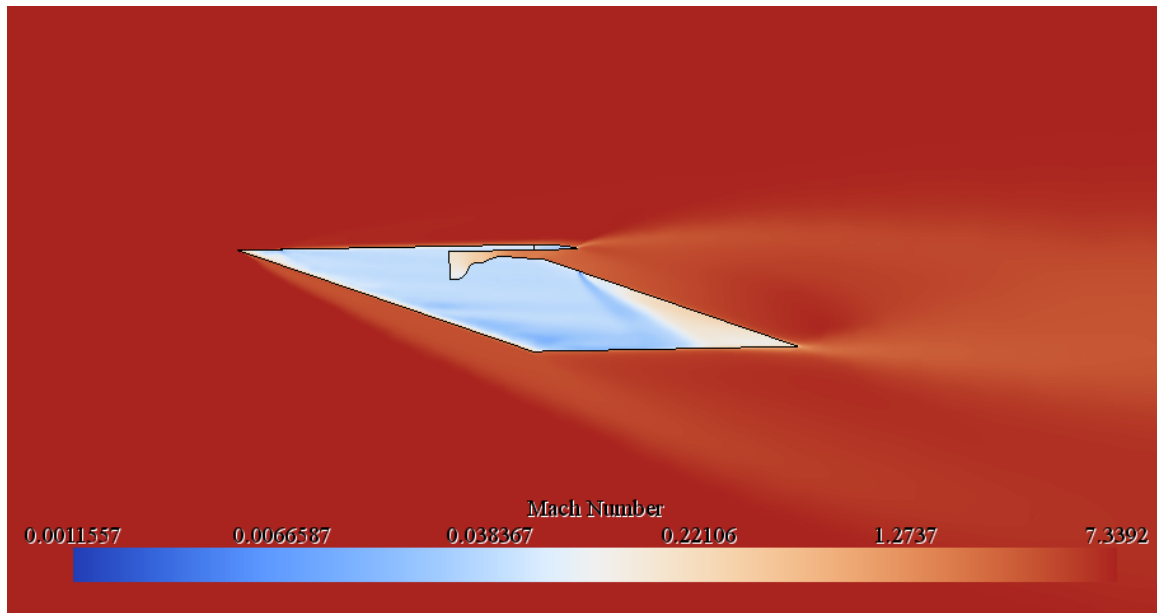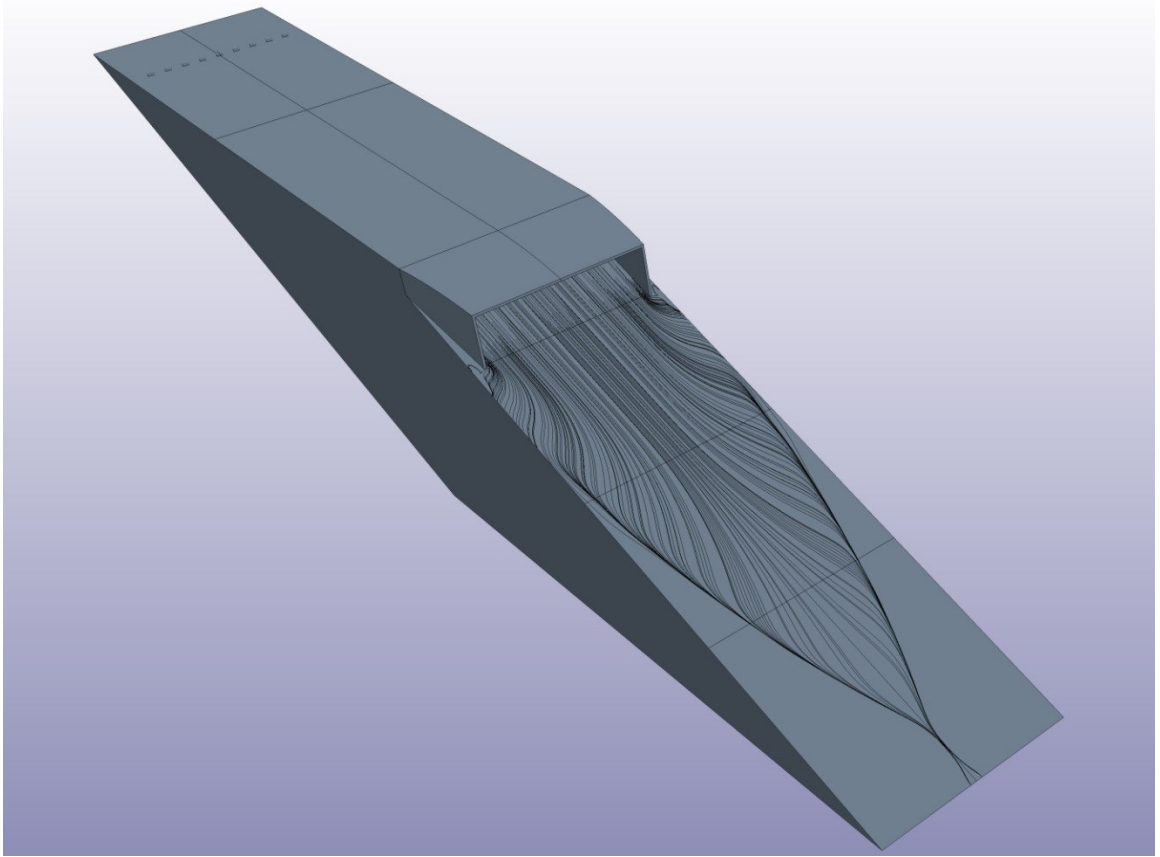
The application of the top-down design methodology to hypersonic vehicle design will be presented in this chapter. A walkthrough of the conceptual and preliminary design stages will be presented for a hypersonic derivative of the Lockheed D-21. The study below is far more limited in scope and less detailed than in an actual design process but is sufficient for the demonstration of the top-down design methodology.

5.1   Vehicle Conceptual Design Stage

The vehicle that is developed in this chapter is the next generation hypersonic research vehicle (NHRV). The NHRV is a conceptual vehicle with the purpose of demonstrating long range hypersonic flight. As such, the vehicle must demonstrate marked improvement over previous generations of hypersonic air-breathing vehicles in terms of range.

The NHRV is based on the geometry of the Lockheed D-21 as a starting point for vehicle development. The Lockheed D-21 is used as a starting point for two reasons. The first reason is to keep the study practical and on target with the goal of merely demonstrating the top-down design methodology rather than developing a completely new vehicle. As such, a proven supersonic vehicle is a much better starting point for this study rather than using some arbitrary geometry.

The second reason is that the D-21 represents an attractive geometry in terms of its aerodynamic performance and static stability at hypersonic speeds. The performance of the vehicle will be discussed in further depth in at the end of subsection 5.1.5. In practice, the selection of the geometry from a candidate pool would occur at the end of the conceptual stage of the design process.

5.1.1   Development of vehicle requirements

As the vehicle is a test bed for hypersonic flight, the philosophy of the vehicle will be to keep its design a simple as possible. In accordance with this philosophy, the NHRV will only be designed for flight in the mid supersonic to low hypersonic range. Additionally, the vehicle will be designed as a single-use air-launched aircraft that will be boosted to supersonic speeds with a rocket booster in the same manner as the original D-21.

This decision results in a number of simplifying consequences. First of all, low speed performance does not need to be considered during the analysis stage. Second, no accommodations for landing and recovery systems such as flaps, landing gears, or parachutes need to be made. Finally, the propulsion system can be simplified considerably as there is no need for any combined cycle engine concepts.

For the weight of the vehicle, an initial gross takeoff weight (GTOW) of 10,000 lbs. is assumed. This roughly corresponds to the gross weight of the D-21 cruise vehicle. The actual gross weight of the D-21 cruise vehicle was 11,200 lb [35]. A vehicle weight similar to that of the D-21 is significant as it means an air drop launch would be feasible. The original D-21 was developed to be dropped from a B-52 and accelerated to cruise

speed by a solid rocket booster [35]. Of the 10,000 lb vehicle gross weight, 1,000 lbs. will be reserved for payload and systems weight.

Initial estimates of fuel were developed by using a correlation Section 3.4 of Raymer's book [9]. Using the correlation for a reconnaissance unmanned aerial vehicle, an empty to gross weight ratio of 0.38 was obtained. This would yield a vehicle empty weight of 3,800 lbs. In order to accommodate the 1,000 lb payload, this ratio was increased to 0.5 which yields a vehicle operational empty weight (OEW) of 5,000 lbs.

5.1.2 Propulsion study

At the edge of the hypersonic flight regime, there are three feasible propulsion systems available: scramjets, ramjets, and rockets. As mentioned in subsection 5.1.1, only a single propulsion system with a solid rocket boost stage will be considered to reduce complexity of the vehicle.

For long range hypersonic cruise vehicles, rockets can effectively be eliminated as an option. Rockets are undesirable due to the necessity to carry both the oxidizer and propellant onboard the vehicle. As a result, the specific fuel consumption of the rocket engine is significantly higher than that of the ramjet or scramjet engines. This leaves only the air-breathing ramjet and scramjet engines as options.

The distinguishing feature of ramjet engines is that the compression stage of the engine takes advantage of ram compression. That is, the vehicle flies at a high enough Mach number that the stagnation pressure rises to a point suitable for combustion. However, the limiting factor on ramjet propulsion is the material and flow temperature limits. If the material of the propulsion path is overheated, structural failure can result.

Gases flowing through the propulsion path may begin to dissociate, reducing the efficiency of the propulsion system.

In conventional ramjet engines, the flow is slowed so that it is subsonic when combustion occurs. However, the issue with this is that as the free-stream Mach number increases, the pre-combustion flow temperature also increases. This can result in dissociation of the combustion products or even dissociation before the flow enters the combustion chamber. The problem of dissociation of combustion products can be solved by increasing the air to fuel ratio (AFR) as the flight Mach number increases. However, pre-combustion dissociation is another issue that is dependent on both the freestream Mach number and the combustion Mach number. Both of these issues effectively limit conventional ramjets to somewhere in the Mach 6 Range [2].

Scramjets are a variation on the conventional ramjet in that combustion occurs at supersonic speeds. Supersonic combustion is advantageous at higher Mach numbers since the static temperature is kept lower. Despite the advantages, scramjet engines have a few practical drawbacks. Scramjets are difficult to start and require either silane or ethylene to be injected into the combustion chamber [36]. Once a scramjet has started, the engine is difficult to keep running. As of this point, the X-51 represents the limit of scramjet powered flight with a flight time of about 200 seconds [36].

Due to the inherent difficulty of getting a scramjet to work, a ramjet propulsion system will be chosen for the NHRV. This choice effectively limits the cruise Mach number to about Mach 6. The fuel of the ramjet will be limited to a hydrocarbon fuel. In particular, JP-10 will be used as the fuel. A refined estimate will for cruise and climb flight paths will be developed in the next section.

5.1.3 Feasible flight envelope

According to Heiser and Pratt, hypersonic air breathing vehicles typically fly in a corridor between 500 and 2000 PSF [2]. Additionally, Heiser and Pratt say that air deviates from a thermally perfect behavior at about 1700 K as dissociation begins [2]. This means that a pre-combustion static temperature of up to 1700 K can be potentially tolerated. Assuming that the pre-combustion Mach number is roughly about 0.1, the total temperature for a given flight Mach number is approximately the same as the static temperature if the flow is decelerated to Mach 0.1. Knowing this, a Mach number limit can be established using the total temperature relation (Eqn. 4.11). Combined, the dynamic pressure and temperature limits establish a feasible flight corridor where the NHRV can fly. Figure 5.1 illustrates the dynamic pressure and temperature limits along with the proposed cruise Mach number.
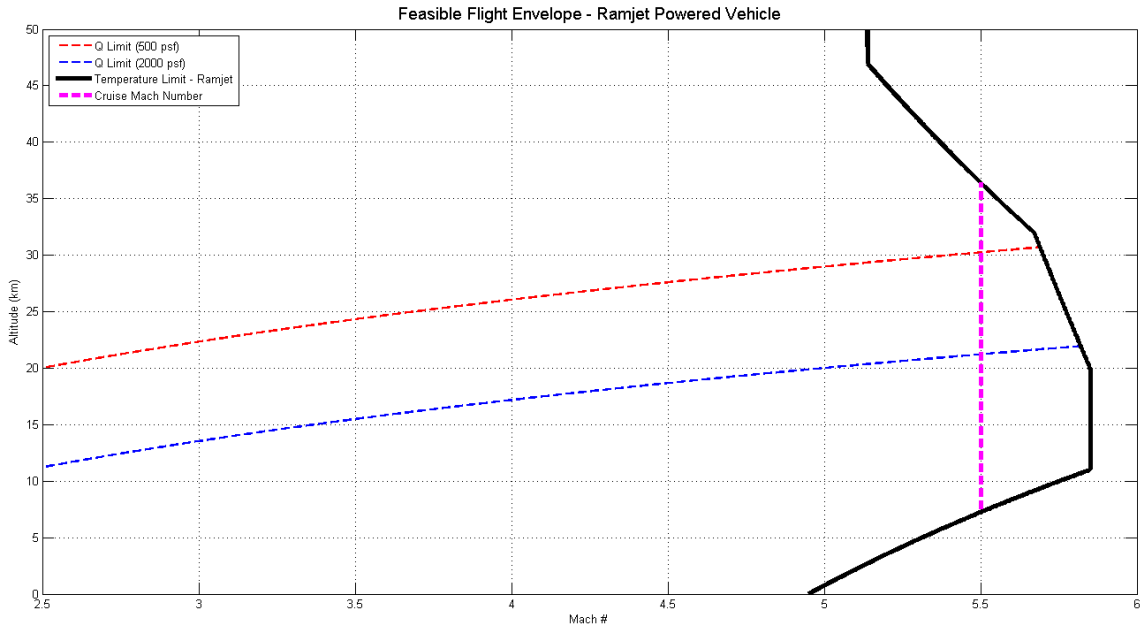

Figure 5.1: Feasible flight envelope of a ramjet powered vehicle

The feasible flight envelope shows that a Mach 5.5 cruise is theoretically feasible between the dynamic pressure limits. However, this chart only displays the temperature limitations of the engine. This chart does not display the net thrust produced by the engine within this flight region.

5.1.4   Initial range trade study

Previous generations of hypersonic vehicles have been somewhat limited in range when compared to conventional aircraft. Arguably, the X-15 represents an historic upper limit of powered hypersonic vehicle with a maximum designed flight distance of 400 nmi. at a maximum flight Mach number of 6.7 [37, 38]. The D-21 had a vastly extended range of approximately 3000 nmi. but was limited to a cruise Mach number of around 3.2 [35]. Striving for a middle ground between these two classes of vehicles would seem like a realistic goal. Therefore, a range of 2,000 nmi will be the chosen goal for the NHRV vehicle.

The feasibility of the 2,000 nmi range for the NHRV is studied by conducting Breguet range study. The study assumed an air-launched vehicle which cruises at Mach 5.5. Additionally, the GTOW of 10,000 lbs. (44,482 N) and OEW of 5,000 lbs. (22241 N) as developed in subsection 5.1.1 are used in this study. A trapped fuel ratio of 1.06 is assumed as recommended by Raymer [9].

Estimates of TSFC are obtained through a theoretical formula derived by Wittenberg [24]. Equations 5.1-5.5 outline the estimation of TSFC as presented by Wittenberg.

$$TSFC = \frac{1}{I_{sp}g_0} \qquad\qquad 5.1$$

$$I_{sp} = \frac{a_0\eta_{tot}\eta_B H_f}{g_0(\gamma-1)M_0 c_p T_0} \qquad\qquad 5.2$$

$$\eta_{tot} = \eta_{th}\eta_j \qquad\qquad 5.3$$

$$\eta_{th} = \frac{1}{1+\dfrac{2}{(\gamma-1)M_0{}^2}} \qquad\qquad 5.4$$

$$\eta_j = \frac{2}{1+\sqrt{\dfrac{T_{t5}/T_0}{1+\dfrac{\gamma-1}{2}M_0{}^2}}} \qquad\qquad 5.5$$

The thrust specific fuel consumption is calculated as the inverse of specific impulse (I_{sp}) and sea-level gravitational acceleration (g_0). It should be noted that in the case of U.S. customary units, g_0 is assumed to be $1\ \frac{ft}{s^2}$ in order to ensure correct unit conversion. η_{tot} represents the total efficiency of the ramjet engine while η_b represents the burner efficiency. η_{tot} is a product of the thermal efficiency η_{th} and propulsive efficiency η_j of the engine. H_f is the lower heating value of the fuel which is 42.1 MJ/kg for JP-10 [39]. M_0, a_0, and T_0 are the freestream Mach number, speed of sound, and static temperature. T_{t5} represents the total temperature limit in the combustion chamber.

The results of the Breguet range study are located in Figure 5.2. The specific fuel consumption estimation predicts a maximum theoretical SFC of 1.39. This means that an L/D of at least 2.8 is necessary in order to meet the target range of 2,000 nmi. However,

this estimate assumes a perfectly efficient ramjet where η_{tot} and η_b are equal to 1. A more realistic estimate assumes a combustion total temperature limit between 2,000 and 3,000 K along with a burner efficiency of 0.85. At the lower end where $T_{t5} = 2000\ K$, a TSFC of 2.02 is predicted. This in turn corresponds to a required L/D of 4.1. At $T_{t5} = 3000\ K$, a TSFC of 2.26 and a required L/D of 4.6 is predicted.

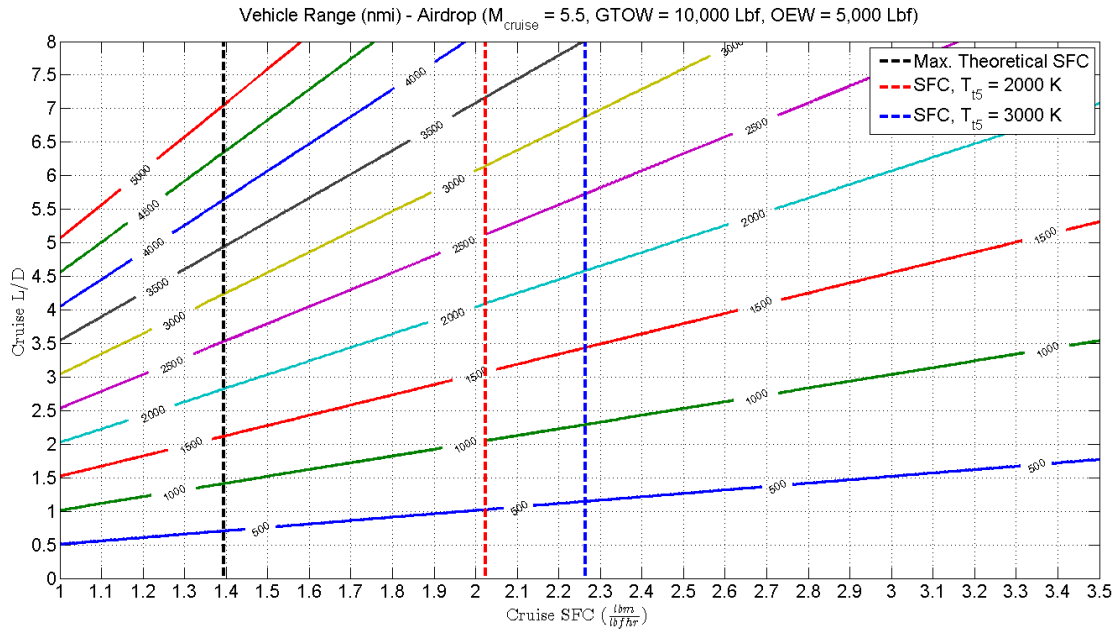Figure 5.2: Range trade study for an air-dropped hypersonic vehicle

5.2   Vehicle Clean-body Evaluation

5.2.1   Vehicle configuration study

The final step of the conceptual design stage in this methodology is to analyze the aero-performance of the prospective vehicle configurations. The clean-body geometry for the D-21 is displayed in Figure 5.3. The inlet and exit to the propulsion path are faired

over so that a generalized aero-performance estimate may be obtained. Table 5.1 contains a list of relevant geometric parameters for the D-21 geometry.

The clean-body aero-performance was evaluated through a set of CFD simulations. The simulations were run at dynamic pressures of 250 PSF, 500 PSF, 1000 PSF, 1500 PSF, and 2000 PSF. The simulations were run at Mach numbers from 2.5 to 5.5 in 1.0 intervals. The exception is at 250 PSF where the simulations were run at Mach number intervals of 0.5. This yields a total of 23 total simulations. Additionally, a simulation included a sweep of angles of attack from 0 to 6 degrees in 2 degree intervals.
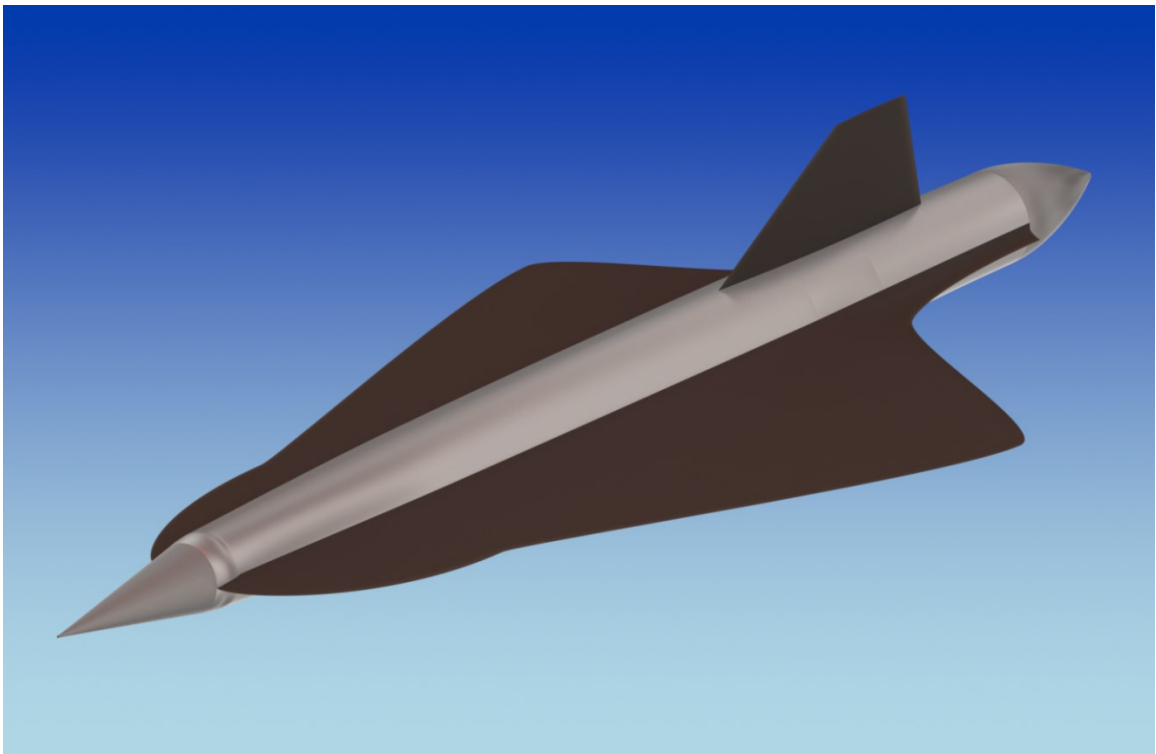

Figure 5.3: CAD model of the D-21 clean-body configuration (CAD geometry courtesy of Alexander Lee)

As L/D is a key parameter of the range of the vehicle, L/D was looked at first. Figures 5.4 and 5.5 illustrate the vehicle L/D as a function of angle of attack and Mach

number. the L/D vs AoA for dynamic pressures of 250 and 2000 psf. This plot
demonstrates is that the max L/D occurs at an angle of attack of 4 degrees for all dynamic
pressures. As expected, minimum L/D occurs at the lowest dynamic pressure.

Table 5.1: D-21 Clean-body configuration geometric parameters

Reference area	43.33 m^2
Vehicle length (with fairings)	15.76 m
Vehicle length (nose fairing only)	14.25 m
Wingspan	6.17 m
Internal volume	13.63 m^3
Wing loading (44,482 N)	$1414.10 \ N/m^2$

As L/D is a key parameter of the range of the vehicle, L/D was looked at first.
Figures 5.4 and 5.5 illustrate the vehicle L/D as a function of angle of attack and Mach
number. the L/D vs AoA for dynamic pressures of 250 and 2000 psf. This plot
demonstrates is that the max L/D occurs at an angle of attack of 4 degrees for all dynamic
pressures. As expected, minimum L/D occurs at the lowest dynamic pressure.

Plots of C_L and C_D vs angle of attack are plotted in Figures 5.6 and 5.7. As
expected, C_L varies little between the 250 PSF and 2000 PSF dynamic pressure
freestream conditions. C_D on the other hand is lower at higher dynamic pressures.
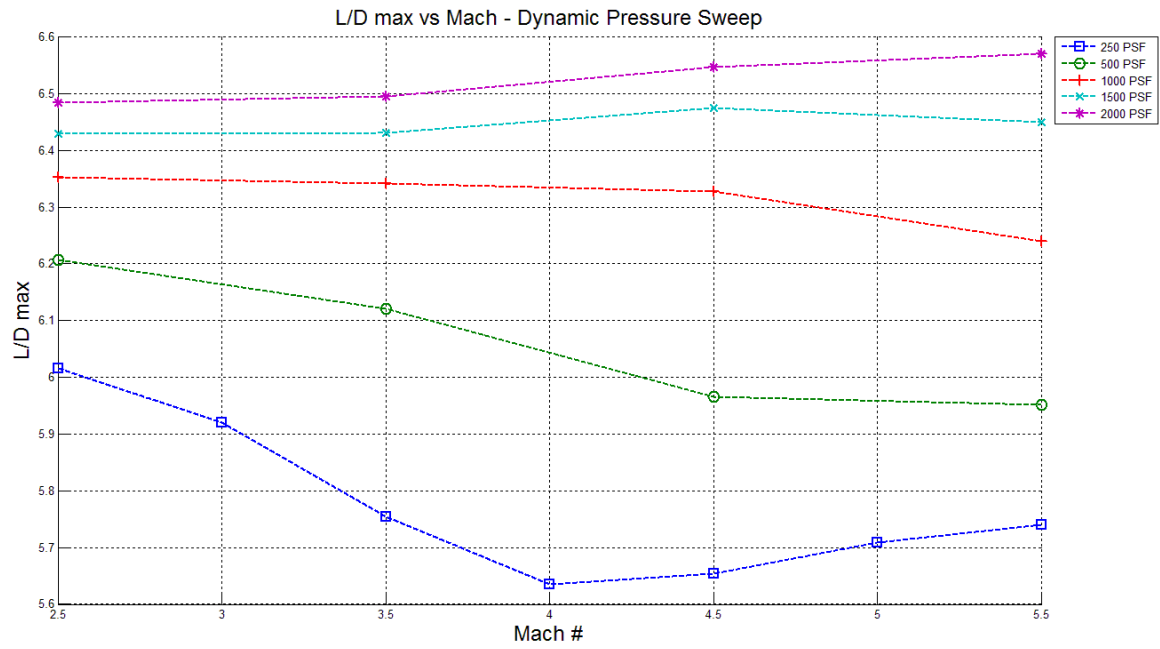
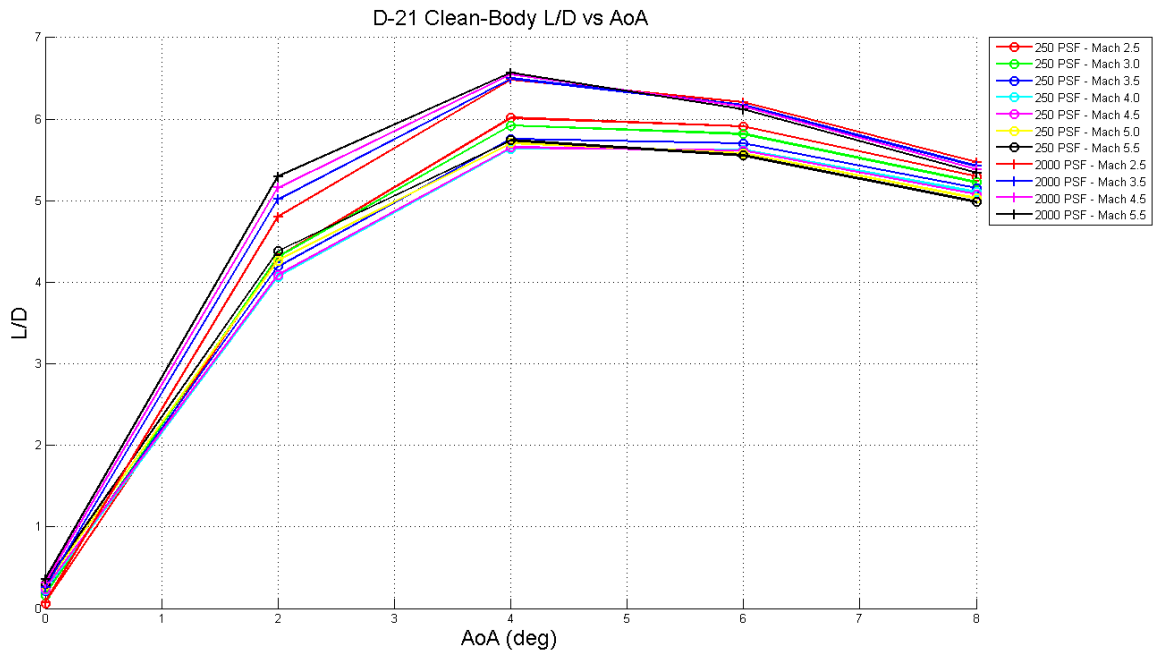Figure 5.4: L/D$_{max}$ vs Mach number for the D-21 clean-body configuration

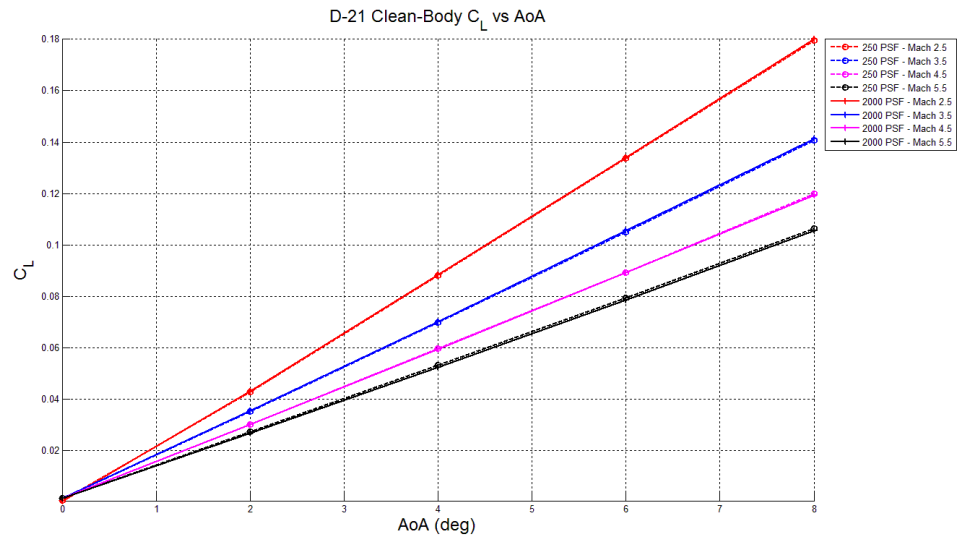Figure 5.5: L/D vs AoA for the D-21 clean-body configuration at 250 and 2000 psf.

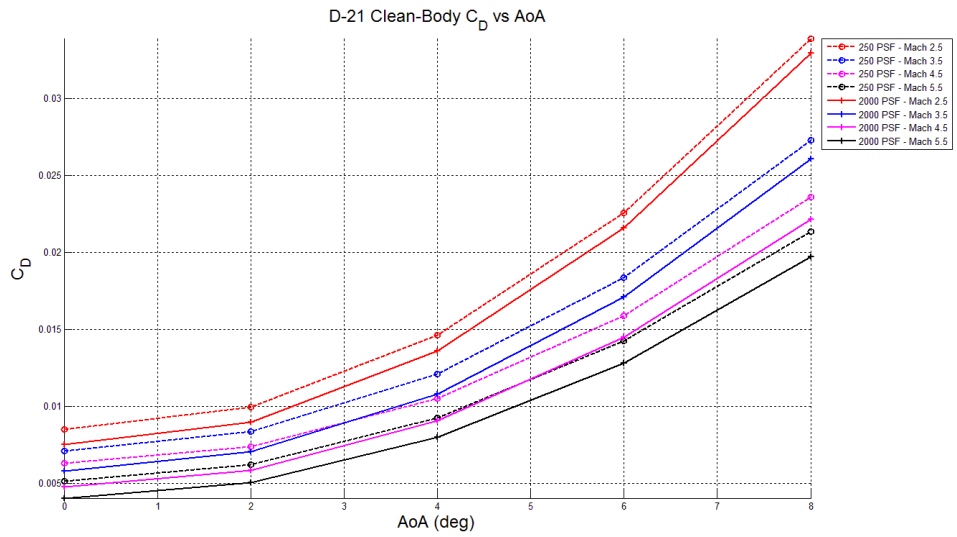Figure 5.6: CL vs AoA for the D-21 clean-body configuration at 250 and 2000 psf.

Figure 5.7: CD vs AoA for the D-21 clean-body configuration at 250 and 2000 psf.

At the cruise Mach number M=5.5, the minimum L/D of 5.74 at 250 PSF and a maximum L/D of 6.57 at 2000 PSF. This data can be used to evaluate the range performance of the configuration. Figure 5.8 expands on the preliminary range trade presented in subsection 5.1.4. This range analysis shows a minimum possible range of 2484 nmi and a maximum possible range of 3180 nmi. Both of these high and low end estimates are significantly higher than the target range of 2000 nmi. However, no propulsion path has been included so these estimates are on the high end.

Ideally, the vehicle should fly at max L/D. By definition, max L/D is the point where the vehicle has the least amount of drag for a given amount of lift. Using the coefficient of lift as a function of Mach number, it is possible to find the Max L/D corridor for the GTOW and OEW of the vehicle. Figure 5.9 superimposes the max L/D corridor over the feasible flight envelope from subsection 5.1.3.
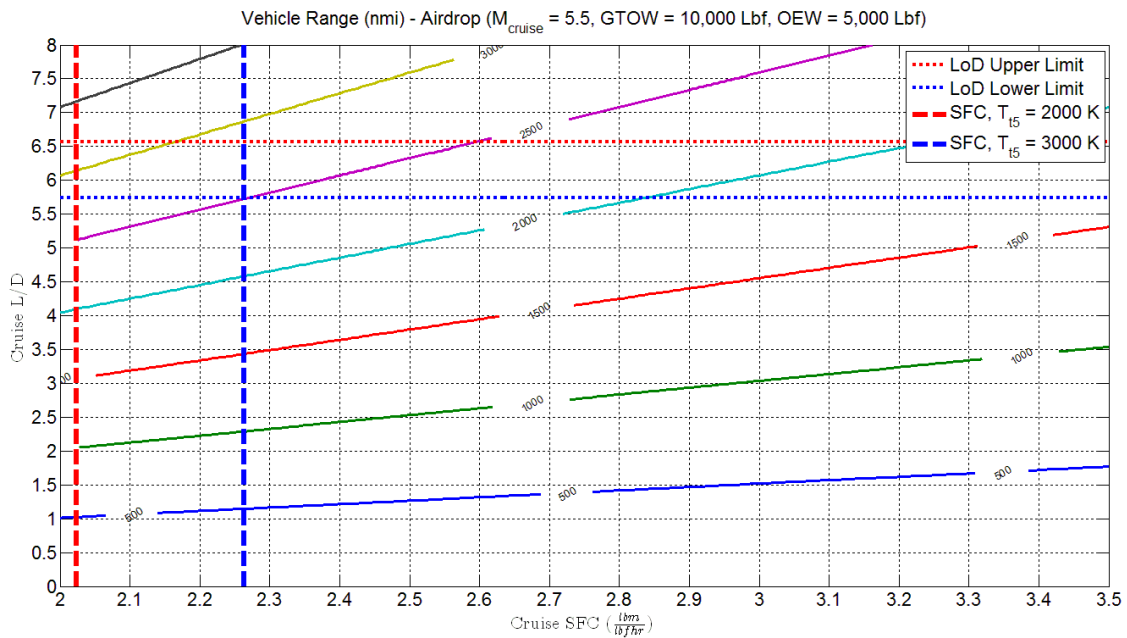
Figure 5.8: NHRV range study
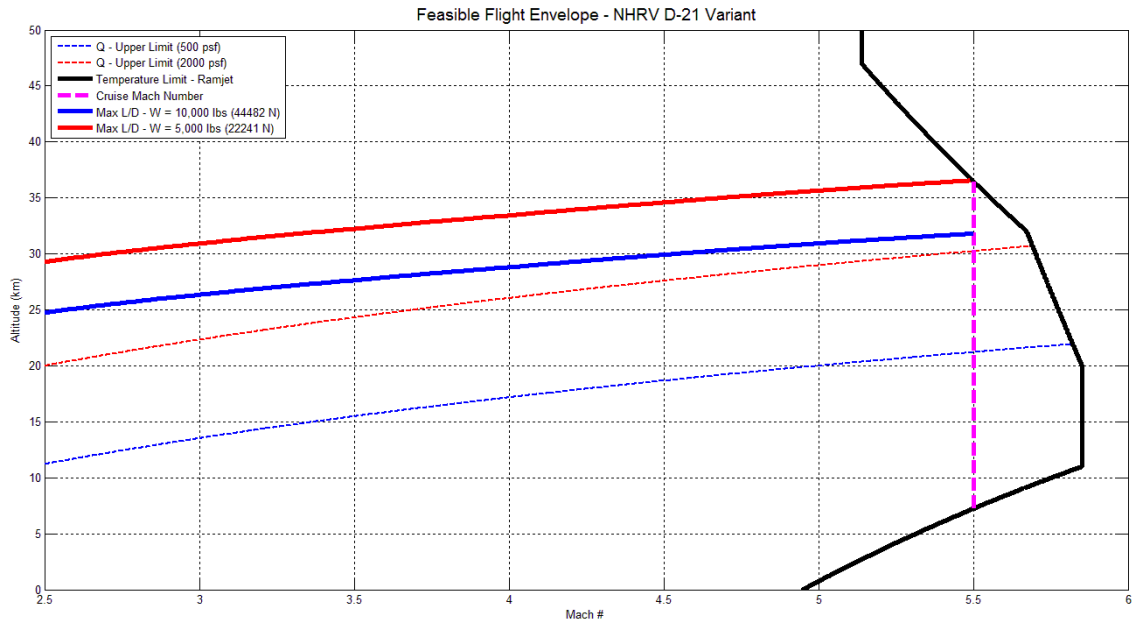
Figure 5.9: NHRV feasible flight envelope

This plot demonstrates that the max L/D corridor is at a much higher altitude than the hypersonic air-breathing corridor according to Heiser and Pratt. This is an early indication that the vehicle airframe may be slightly oversized or the vehicle is underweight for the given airframe size.

5.2.2 Fuel selection

JP-10 fuel was chosen as the fuel for the NHRV due to its previous use in other ramjet powered vehicles [27]. A study was conducted in order to determine at which temperature the combustion chamber would begin to produce significant amounts of an undesirable species. A significant quantity of a species was defined in this study as any species that made up more than 1% of the total mass of the combustion products. The 1% limitation is significant as this is roughly the mass percentage of Argon in the atmosphere

[25]. Argon was neglected in this study in order to simplify CFD computation by reducing the amount of species accounted for.

Using the NASA CEA calculator, combustion products were calculated for a temperature range of 1750 K to 3000 K in intervals of 250 K and at static pressures of 80.97 kPa and 1,806 kPa. The results of these analyses show that N_2, CO_2, and H_2O are the only significant species up to a temperature of roughly 2250 K. As such, the temperature of the combustion chamber is limited to a maximum temperature of 2250 K.
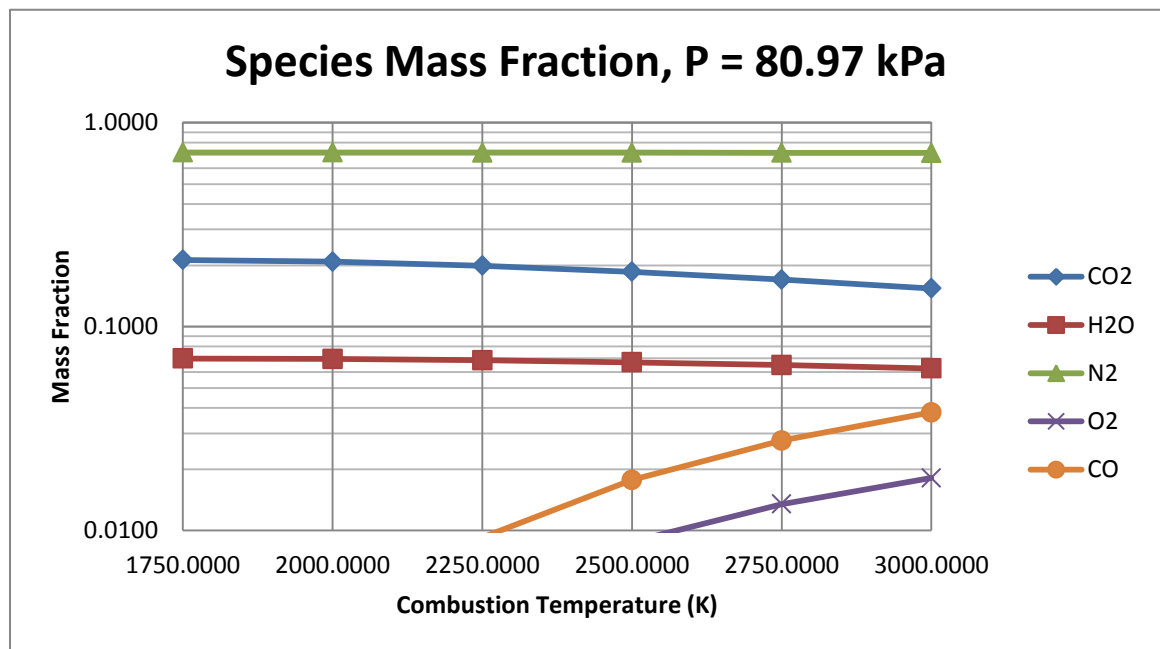
Figure 5.10: Post-combustion species at minimum combustor static pressure
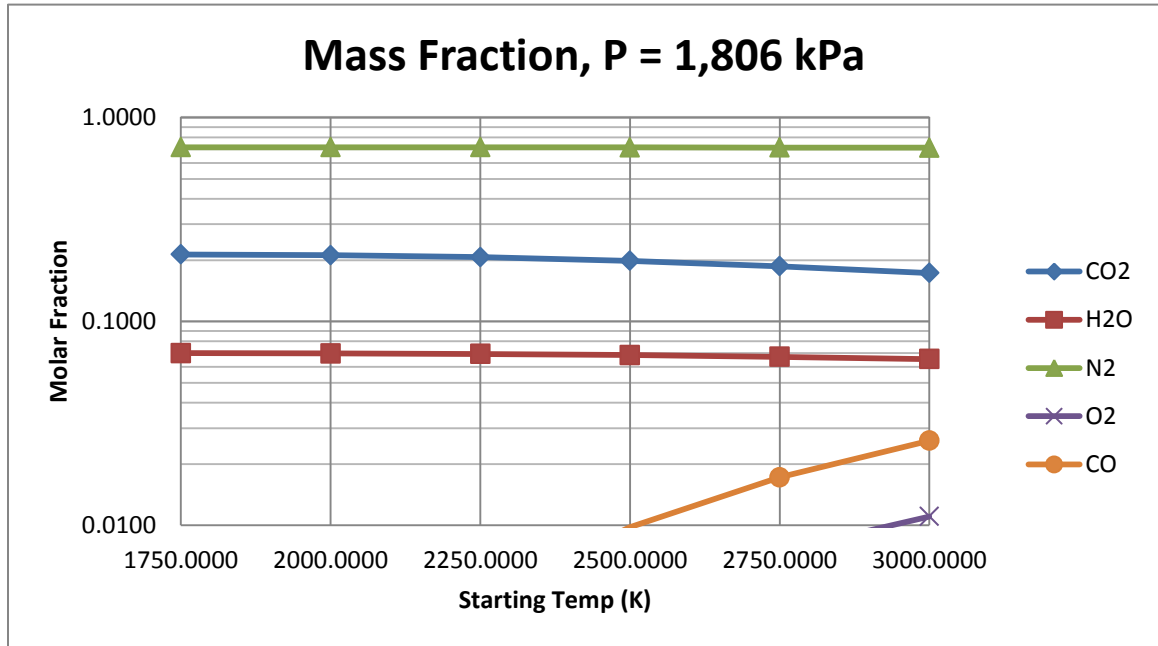
Figure 5.11: Post-combustion species at maximum combustor static pressure

5.2.3   Optimal Trajectory

Having obtained aerodynamic data for the clean-body, the calculation of the optimal trajectory can be conducted. As mentioned in the last section, a combustion temperature of about 2250 K could be achieved before dissociation occurs. Assuming this combustion temperature, Equations 5.1-5.5 were once again used to calculate TSFC as a function of Mach number. The results of the optimal trajectory analysis are shown in Figure 5.12.

This analysis showed that a minimum thrust to weight ratio of 0.20 was necessary in order to reach a cruise Mach of 5.5. Furthermore, Table 5.2 shows that there is a point of diminishing returns where an increase in the thrust to weight ratio yields only an insignificant increase in range.

Figure 5.12: Optimal range analysis for the D-21 clean-body configuration

Table 5.2: Range vs T/W D-21 clean-body configuration

T/W	Range
0.20	4929.51 nmi
0.25	5478.61 nmi
0.30	5588.57 nmi
0.40	5654.43 nmi

This point occurs at a thrust to weight ratio of greater than 0.3. Therefore, the target thrust to weight ratio of the vehicle will 0.3. Assuming a perfectly expanded nozzle, the ide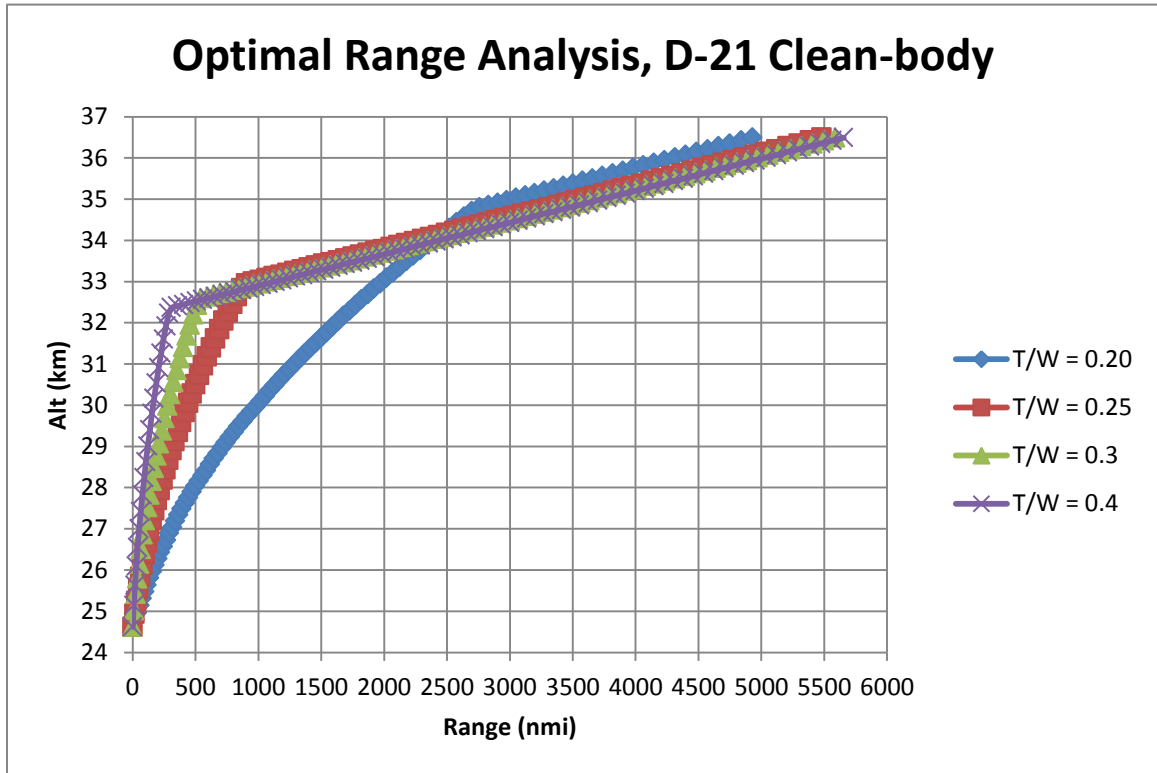al ramjet cycle analysis can be used to obtain an approximate sizing of the ramjet engine. The results of this analysis are in Table 5.3.

Table 5.3: Ideal cycle analysis of optimal trajectory

Flight Mach	Altitude (km)	Range (nmi)	Thrust (N)	$\dot{m}$ (kg/s)	Capture Area (m^2)
2.5	24.62	0.00	13344.00	15.11	0.48
3.0	26.51	66.70	13010.40	15.06	0.53
3.5	27.83	133.21	12744.52	15.78	0.58
4.0	29.07	211.37	12477.64	17.25	0.67
4.5	30.27	300.87	12210.76	19.79	0.82
5.0	31.41	401.52	11943.88	24.2	1.08
5.5	32.60	542.80	11609.28	32.88	1.60
5.5	36.50	5588.57	6605.28	21.39	1.86

5.3   Vehicle Preliminary Design

With the overall vehicle performance evaluated and the conceptual design stage concluded, the preliminary design stage can begin. The preliminary design stage focuses on the introduction of system level components into the vehicle model. The integrated development of the propulsion system is presented in this section.

5.3.1   Initial propulsion path integration

For the first integrated nozzle configuration, a cone nozzle (pictured in Figure 5.13) was chosen as a starting point. This is due to the relative simplicity of the cone nozzle

design and the fact the straight geometry is less likely to create efficiency reducing shocks within the nozzle. The efficiency and simplicity of the cone nozzle does come at the cost of additional weight when compared to other nozzles such as the bell nozzle.
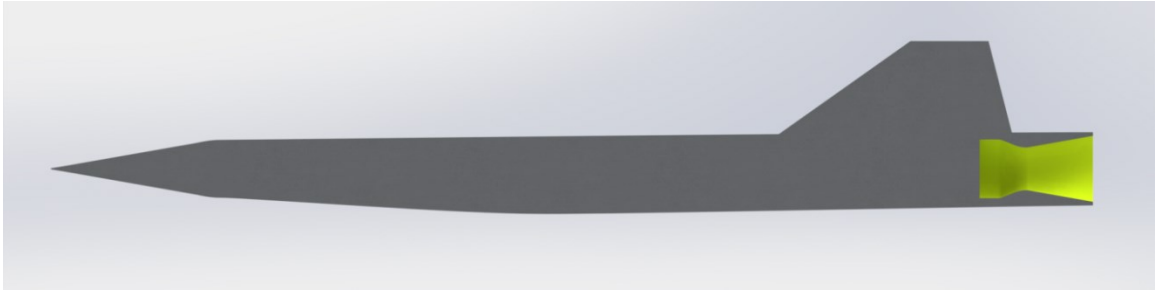
Figure 5.13: CAD geometry of the cone nozzle variation of the D-21

The nozzle was developed with a low area ratio in order to ensure that the nozzle was never over-expanded in the potential flight regime. The potential consequence of an over-expanded nozzle would be flow separation in the nozzle due to an adverse pressure gradient. The nozzle was meant to match freestream static pressure at the flight condition of Mach 2.5 at 2000 PSF. This represents the point of highest freestream static pressure in the potential flight regime.

Table 5.4: Post-combustion parameters for
(Mach 2.5, 2000 PSF.)

γ	1.2492
P_∞	21.89 kPa
P_{comb}	319.69 kPa
$P_{t,comb}$	321.91 kPa
T	2346.25 K
$T_{t,comb}$	2372.57 K

Table 5.4 lists the post-combustion flow parameters as calculated by the ramjet cycle program for the Mach 2.5, 2000 PSF case. Using a calorically perfect assumption, a nozzle was created in order to match freestream static pressure at this flight point. Relevant geometrical parameters of this initial cone nozzle are listed in Table 5.5.

Table 5.5: Cone nozzle variant parameters

A_{exit}/A^*	2.39
A_{exit}	0.64 m^2
Cone Angle	10.00 deg.

5.3.2 Combined performance of aeroshell and propulsion path for the cone nozzle variation

The performance of the nozzle was evaluated over the entire potential flight range. This flight range spanned from Mach numbers of 2.5 to 5.5 and dynamic pressure of 500 Psf. to 2000 Psf. The flight range was then discretized in Mach number intervals of 1 and dynamic pressure intervals of 500 Psf. This created a set of 16 analysis point in the flight range. Additionally, the vehicle was analyzed at angles of attack of 0 to 6 degrees in intervals of 2 degree.

A plot of the Max L/D in Figure 5.14 shows between a 13 to 19% increase in the max L/D of the vehicle as compared to the clean-body configuration. This demonstrates that the addition of the propulsion path has a significant effect on reducing the base drag of the vehicle.
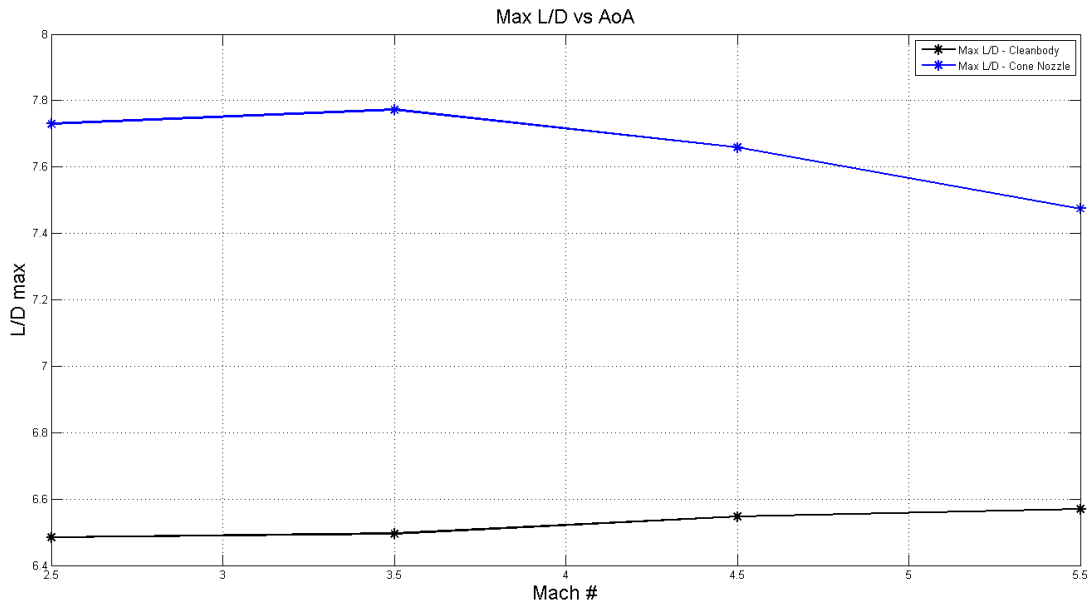
Figure 5.14: Comparison of Max L/D between clean-body and cone nozzle configurations

The results of the simulations show that the maximum inlet area imposes a limitation on the flight envelope of the vehicle. As the total pressure in the combustion chamber increases, the choked mass flow rate of the nozzle also increases. However, the maximum mass flow rate is limited by the maximum area of the inlet. The maximum inlet area of the NHRV D-21 vehicle is $0.3959\ m^2$. Figure 5.15 shows the required inlet capture area as a function of both Mach number and dynamic pressure. As demonstrated by this figure, the maximum flight Mach number of the NHRV is limited to just under Mach 3.

Figures 5.16 and 5.17 illustrate the thrust to weight ratio for the vehicle at gross takeoff and operational empty weights. These figures show that the thrust to weight ratio exceeds 1.0 which means that the vehicle is capable of vertical flight. Vertical flight is neither necessary nor desired for the NHRV hypersonic test bed mission.
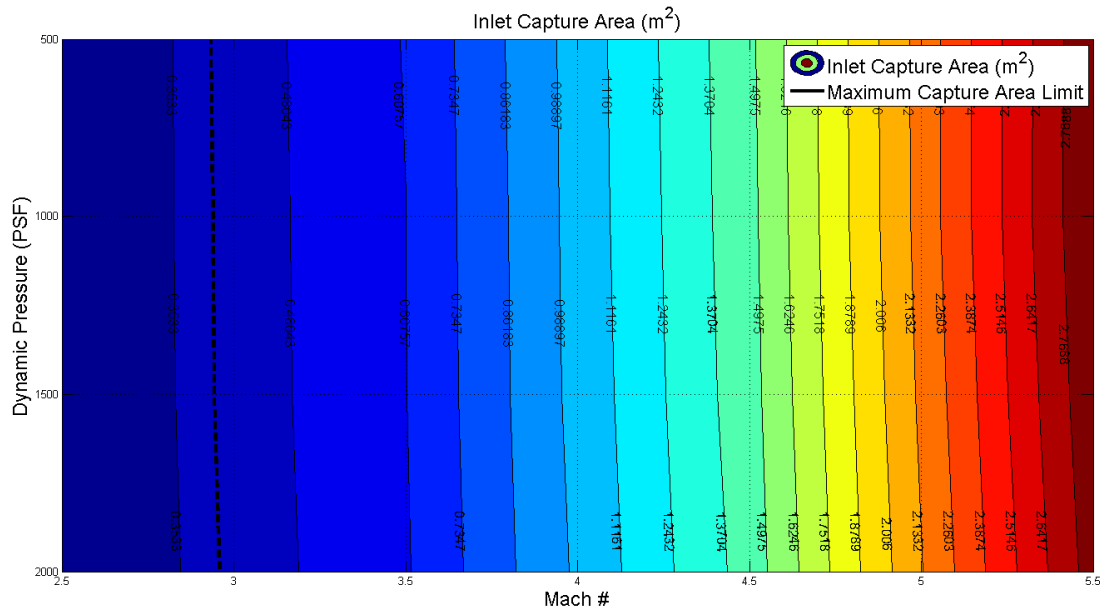
Figure 5.15: Inlet capture area
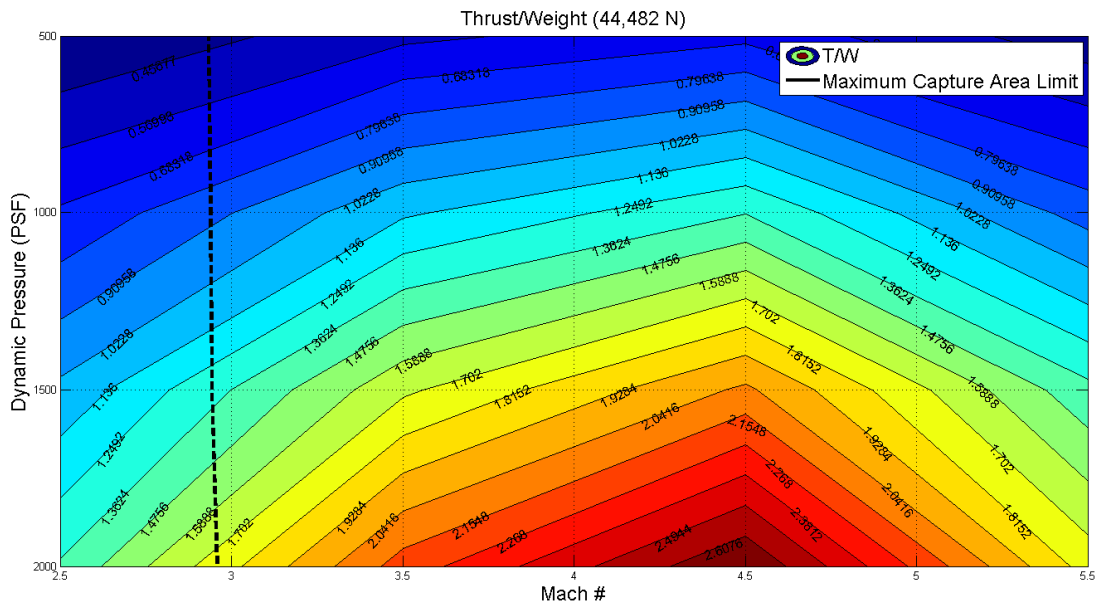
Figure 5.16: Thrust to Weight ratio at Gross Takeoff Weight
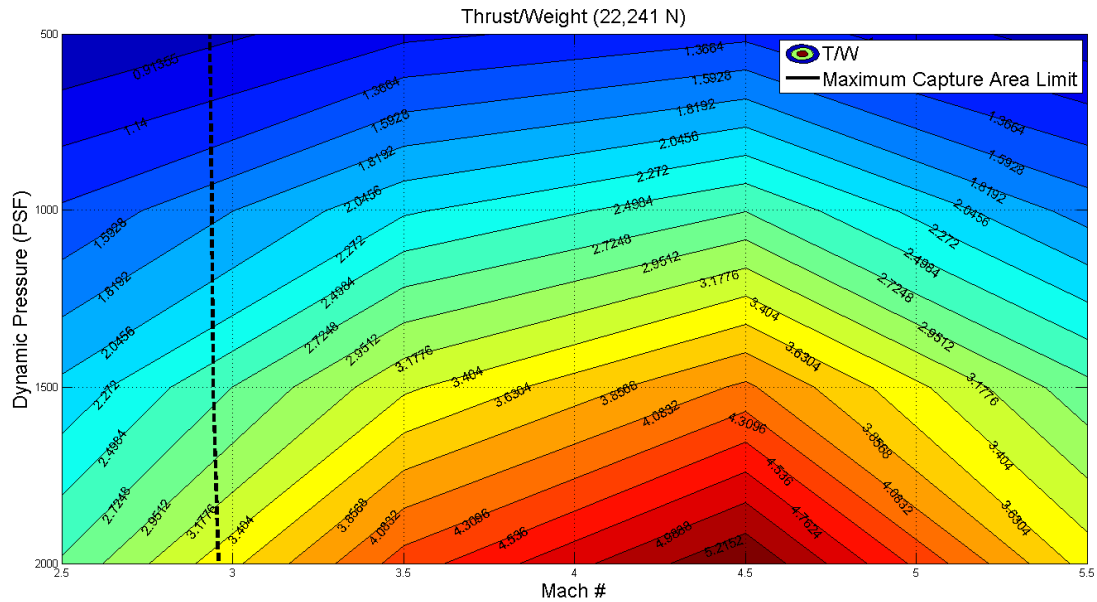
Figure 5.17: Thrust to Weight ratio at Operational Empty Weight

Based on the available data from these simulations, a trajectory was calculated using the optimal trajectory method. The trajectory was calculated up to a cruise Mach number of 2.9 as the inlet limited the vehicle prevented the vehicle flying at any higher speeds. The thrust to weight ratio was also assumed to be held at 0.3 for the climb portion of the flight. The results of this range analysis are shown in Figure 5.18. A range of 3861.16 nmi was calculated for the initial nozzle configuration.
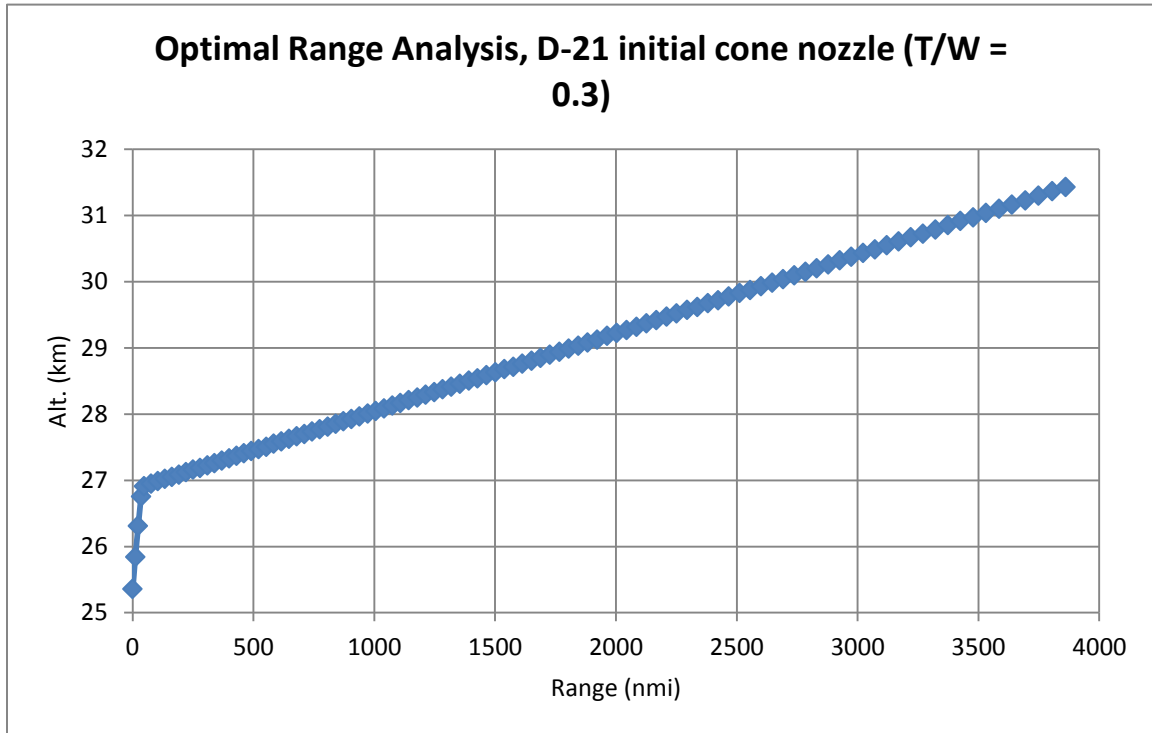
Figure 5.18 : Optimal range analysis for the D-21 initial cone nozzle

From the analysis of the initial cone nozzle, a set of recommendations were developed. First, it is recommended that the throat area of the nozzle be reduced. The required capture area for the initial nozzle concept far exceeded the actual cross sectional area of the fuselage. Additionally, the thrust produced by the engine is far in excess of what is necessary for the NHRV mission. The thrust of the engine is directly proportional to the mass flow rate of air through the engine.

5.3.3   Analysis of second iteration nozzle concepts

As the initial cone nozzle concept proved inadequate, a second design iteration was conducted. This second iteration consisted of an improved cone nozzle, a bell nozzle, and a double bell nozzle. Geometric parameters of the three nozzles are featured in Table 5.6. Rather than using the full Mach number and dynamic pressure sweep, these nozzle

concepts were analyzed at only 250 PSF and Mach numbers of 2.5 and 5.5. Additionally, only one angle of attack was analyzed for each variation. This angle of attack was the max L/D angle of attack which coincided at 4 degrees for all of the variations.

Table 5.6: Geometric properties of the second iteration nozzle configurations

Configuration:	Exit area (m^2):	Area ratio	Nozzle surface area (m^2)
2nd cone nozzle	0.6362	28.66	1.926
Bell nozzle	0.6362	28.66	1.343
Double bell nozzle	0.6362	28.66	1.488

The nozzles were designed with a smaller throat and higher area ratio. All of the nozzles had a throat area of 0.02217 m^2 which is roughly 10% of the throat area of the first iteration cone nozzle. This would have the effect of significantly reducing the thrust and thrust to weight ratio in comparison to the first iteration nozzle. All of the nozzle concepts also had an area ratio of 28.66. The nozzle area ratios were increased from the first iteration in order to fly at the higher altitudes of the optimal L/D trajectory.

Table 5.7: Weight properties of the second iteration nozzle configurations

Configuration:	Nozzle weight (N)	Weight change from baseline (N)	GTOW (N)	OEW (N)
2nd cone nozzle (baseline)	906.7	N/A	44480	22240
Bell nozzle	632.2	-274.5	44210	21970
Double bell nozzle	700.6	-206.2	44270	22030

The CFD analyses were used to perform an optimal range analysis of each of the nozzle concepts. Difference in aerodynamic performance in terms of lift and drag of each of the concepts were insignificant between the variations. As a result, the differences in trajectories of each of the concepts are due solely to the differences in propulsive performance and nozzle weight reduction. Table 5.8 presents the thrust and specific fuel consumption for each of the nozzle concepts at Mach 2.5 and 5.5.

Table 5.8: Thrust and specific fuel consumption of the second iteration nozzle
configurations

Configuration:	Thrust, M = 2.5 (N)	Thrust, M = 5.5 (N)	TSFC, M = 2.5 (Lb./Lbf.*hr)	TSFC, M = 5.5 (Lb./Lbf.*hr)
2nd cone nozzle (baseline)	605.2	1707	2.187	2.171
Bell nozzle	997.1	2235	1.327	1.747
Double bell nozzle	554.3	2358	2.569	1.579

A sweep of thrust to weight ratios was conducted for the optimal trajectories. A thrust to weight ratio of 0.3 was again found to be the point of diminishing returns for the maximum range of the vehicle. The results of the optimal range analysis are shown in Figure 5.19.

The double bell nozzle is the most promising of the three designs with a range of 9124 nmi. The bell nozzle has a slightly reduced range of 8672 nmi. However, it should be noted that the optimal range analysis assumes that the vehicle can supply enough thrust to maintain a thrust to weight ratio of 0.3 along the trajectory.
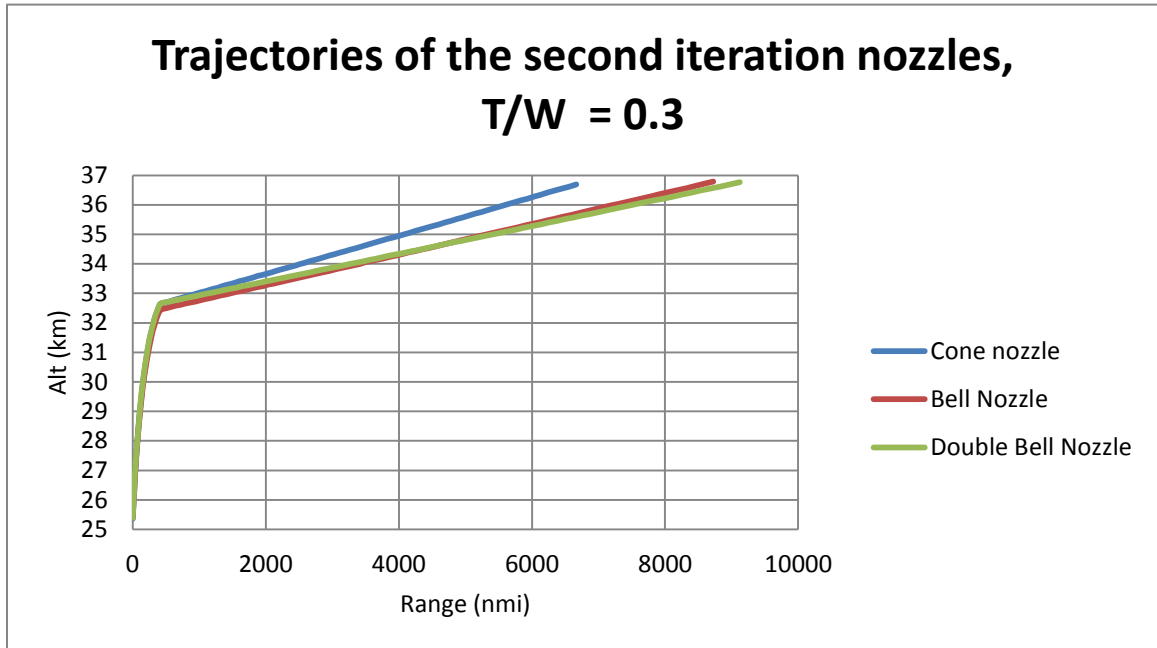
Figure 5.19: Optimal trajectories of the second iteration nozzle configurations

An analysis of surplus thrust is shown in Figure 5.20 and demonstrates a significant thrust deficit for all the nozzle concepts. This thrust deficit is especially prominent at the lower Mach numbers. The analysis also demonstrates that while the double bell nozzle may have the greatest potential range, the bell nozzle has the lowest thrust deficit of the nozzle concepts.

From the second iterations analysis, several conclusions can be drawn. First, the nozzle throat needs to be increased. The throat size was reduced too much from the first iteration. The second conclusion is that the cone nozzle is deficient in thrust, efficiency, and weight for the purposes of the NHRV design. Therefore, future iterations should concentrate on the bell and double bell nozzle designs.

Figure 5.20: Thrust surplus of the second iteration nozzles

CHAPTER 6. DISCUSSION OF RESULTS

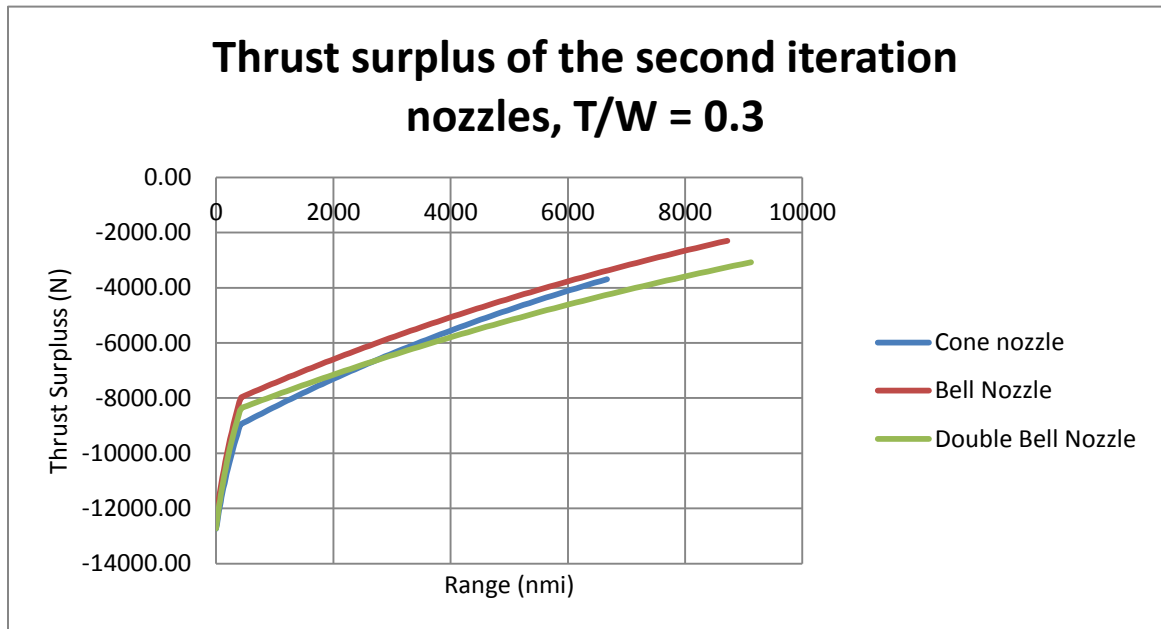An evaluation of the top-down design methodology is presented in this section. The evaluation of the design process includes discussing the strengths and weakness, the computational cost, and the potential pitfalls of the methodology.

6.1 Computational Analysis

After the computational analysis portion of this study, several observations were made on the results produced. The first result to note from the computational analysis was the low reported values for TSFC of vehicle concepts. This is likely due to the ideal assumptions made for the inlet and combustor sections of the ramjet. The inlet and combustor sections are expected to be included in future analyses which will likely result in an improved fuel consumption calculation.

The second note is on the use of viscous CFD simulations. The most noticeable effect of including viscous flow is on the drag accounting of the vehicle. To demonstrate, the viscous drag compared to the total drag was evaluated at the zero lift angle of attack. For the clean-body configuration, the viscous drag made up between 37.3% and 55.4% of the total drag. For the cone nozzle configuration, viscous drag made up between 42.1% and 60.6% of the total drag.

6.2 Computational Cost

Simulations were run six at a time on two computers. Parallel processing was used so 5 processes were dedicated for each simulation resulting in 15 processes used on each computer. For the clean-body CFD simulations, 8.62 hours was spent on average per angle of attack. This means that a standard 4 data point angle of attack sweep for a clean-body simulation would take 34.48 hours. Thus, a series of simulations ranging from 500 to 2000 PSF and 2.5 to 5.5 Mach number (16 total aoa sweeps) could take 103.44 hours or roughly four and a half days to complete.

The later propulsion path simulations took longer to solve at 17.1 hours on average per angle of attack to fully converge. An angle of attack sweep consisted of four angles of attack which would have resulted in a total computational time of 68.4 hours per sweep. A series of simulations ranging 500 to 2000 PSF and 2.5 to 5.5 Mach number (16 total aoa sweeps) could take 205.2 hours or roughly eight and a half days to complete.

6.3 Data Management

At this point, data management is a weakness of the top-down design methodology. Star CCM+ lacks any native method to export reports in the form of text files. As a result, data export is limited to either by-hand processing or 3rd party written data processing codes. In this study, post-processing for a given dynamic pressure and Mach number was conducted by recording lift, drag, moment, and thrust data versus iteration and exporting this into a CSV file. The data was then copy and pasted manually from the CSV file to a pre-made Excel report file for that given dynamic pressure and Mach number. Plots as

shown in subsection 5.3.2 were generated by a Matlab program that processed that data

contained in the Excel files.

CHAPTER 7.   CONCLUSIONS

This study has demonstrated the top-down design methodology as applied to the development of hypersonic vehicles. As mentioned previously in this paper, there were two main objectives of this study. The first objective of this paper was to discuss the top-down design methodology and to demonstrate its application. The second objective was to evaluate the methodology and develop a list of benefits and drawbacks to using the top-down design methodology.

In the first chapters of the paper, the origins of the top-down methodology along with the details of the methodology were discussed. The distinguishing feature of the top-down design methodology is the introduction of high fidelity tools early on to evaluate fully integrated CAD models. As such, a discussion of these tools was also necessary. As there is always an uncertainty associated with using computational tools for design, a validation case was chosen to compare experimental and computational results. The result of this validation case established some level of confidence in the computational tools used.

The evaluation of the methodology showed that despite the promises of the top-down methodology, there are still some significant drawbacks to the system that need to be addressed before it can be implemented. The benefits of applying this methodology include the calculation of effects such as shear drag and the ability to add species to the flow for a better calculation of the ratio of specific heats.

The main disadvantages of this methodology were the computational cost of each simulation. Iteration time for a single propulsion path design could take a maximum of 16 days assuming one computer or eight days assuming two. An issue like this could be circumvented by running simulations in a batch mode on a server. However, it should be noted that convergence difficulty was encountered for these simulations. This may result in difficulties in processing batch mode simulations.

Once the difficulties have been resolved, the top-down design methodology could be expanded to include disciplines such as structures, flight dynamics, and controls. Both flight dynamics and controls could currently be implemented with Star CCM+. Star CCM+ allows both static and dynamic simulations which in turn allow the calculation of static and dynamic stability of the vehicle. Control studies could also be easily implemented by adding parameterized control surfaces to the CAD model. At the present time, structures would require the addition of an additional analysis program.

BIBLIOGRAPHY

[1]   J. D. Anderson, Jr., "Hypersonic and High Temperature Gas Dynamics," ed. New York: McGraw-Hill, 1989, pp. 13-24.

[2]   W. H. Heiser and D. T. Pratt, *Hypersonic Airbreathing Propulsion*: American Institute of Aeronautics and Astronautics, 1994.

[3]   T. A. Barber, B. A. Maicke, and J. Majdalani, "Current State of High Speed Propulsion: Gaps, Obstacles, and Technological Challenges in Hypersonic Applications," presented at the 45th AIAA/ASME/SAE/ASEE Joint Propulsion Conference & Exhibit, Denver, Colorado, 2009.

[4]   K. G. Bowcutt, "A Perspective on the Future of Aerospace Vehicle Design," presented at the 12th AIAA International Space Planes and Hypersonic Systems and Technologies, Norfolk, Virginia, 2003.

[5]   P. Perrier, B. Stoufflet, P. Rostand, V. K. Baev, A. F. Latypov, V. V. Shumsky*, et al.*, "Integration of an hypersonic airbreathing vehicle: assesment of overall aerodynamic performances and of uncertainties.," presented at the AIAA Sixth International Aerospace Planes and Hypersonics Technologies Conference, Chattanooga, TN, 1995.

[6]   M. Tang and R. Chase, "Hypersonics - A Periodic Quest," presented at the AIAA/CIRA 13th International Space Planes and Hypersonics Systems and Technologies, Capua, Italy, 2005.

[7]   L. M. Nicolai and G. E. Carichner, "Fundamentals of Aircraft and Airship Design: Volume 1 - Aircraft Design," J. A. Schetz, Ed., ed. Reston, Virginia: AIAA, 2010, pp. 23-26.

[8]   M. Asimow, "Introduction to Design ", ed. Englewood Cliffs, N.J.: Prentice Hall, 1962.

[9]   D. P. Raymer, "Aircraft Design: A Conceptual Approach," 5th Edition ed. Reston, Virginia: AIAA, 2012, pp. 9-25.

[10]   P. M. Institute, "A Guide to the Project Management Body of Knowledge (PMBOK® Guide) - Fifth Edition," ed, 2008.

[11]   J. E. Hirsh, J. B. Wilkerson, and R. P. Narducci, "An Integrated Approach to Rotorcraft Conceptual Design," presented at the 45th AIAA Aerospace Sciences Meeting and Exhibit, Reno, Nevada, 2007.

[12]   M. A. Ahlqvist, J. F. Nayfeh, and P. R. Zarda, "Designing and Optimizing Missiles in an Interactive Environment," presented at the 9th AIAA/ISSMO Symposium on Multidisciplinary Analysis and Optimization, Atlanta, Georgia, 2002.

[13]   J. S. Robinson, "An Overview of NASA's Integrated Design and Engineering Analysis (IDEA) Environment," presented at the 17th AIAA International Space Planes and Hypersonic Systems and Technologies Conference, San Francisco, California, 2011.

[14]   "The Adaptive Modeling Language. A Technical Perspective," ed: TechnoSoft Inc., 2003.

[15]   P. Perrier and P. Rostand, "Hypersonic airbreathing aircraft integration through CFD: Global Simulations for global thinking," presented at the AIAA/SAE/ASME/ASEE 30th Joint Propulsion Conference and Exhibit, Indianapolis, IN, 1994.

[16]   K. G. Bowcutt, G. Kuruvula, T. A. Grandine, T. A. Hogan, and E. J. Cramer, "Advancements in Multidisciplinary Design Optimization Applied to Hypersonic Vehicles to Achieve Closure," presented at the 15th AIAA International Space Planes and Hypersonic Systems Systems and Technologies Conference, Dayton, Ohio, 2008.

[17]   P. Wilhelm, P. Leyland, P. Jaussi, R. Wiesendanger, A. Ivanov, L. Gathier, *et al.*, "Integrative Design Loop for the Preliminary Study of a Suborbital Transportation System," presented at the 29th AIAA Applied Aerodynamics Conference, Honolulu, Hawaii, 2011.

[18] T. Gielda, "The Role of Simulation-Based Design in Systems Engineering," presented at the Department of Defense High Performance Computing Modernization Program, Portland, Oregon, 2011.

[19] D. Schoon. (August 26). *Top-Down Modeling in Solidworks*. Available: http://web.mit.edu/2.009/www/resources/mediaAndArticles/Solidworks_topDown.pdf

[20] T. Gielda, "Iowa State University Aerospace Engineering 461/462 Class Notes," ed, 2014.

[21] A. Lee, "Parametric modeling for simulation based hypersonic vehicle design," Master's of Science, Department of Aerospace Engineering, Iowa State University, 2014.

[22] A. E. J. Bryson, M. N. Desai, and W. C. Hoffman, "Energy-State Approximation in Performance Optimization of Supersonic Aircraft," *Journal of Aircraft,* 1969.

[23] "Star CCM+ Version 9 Manual," ed: CD-adapco.

[24] H. Wittenberg, "Some Fundamentals on the Performance of Ramjets with Subsonic and Supersonic Combustion," ed. Delft, Netherlands: TNO Prins Maurits Laboratory, 2000.

[25] "U.S. Standard Atmosphere, 1976," NOAA, NASA, and USAF, Eds., ed, 1976.

[26] J. Corish, "What is the difference between generalized cylinder and extruder meshers? Which model should I use?," ed: CD-Adapco, 2013.

[27] T. A. Ward, *Aerospace Propulsion Systems*. Singapore: John Wiley & Sons, 2010.

[28] J. D. Anderson, "Fundamentals of Aerodynamics," 4th ed: McGraw Hill Higher Education, 2007.

[29] "General Specification for Engines, Aircraft, Turbojet and Turbofan," vol. Military Specification MIL-E-5007D, ed, 1973, pp. 12-13.

[30] NASA. (2010, April 25th). *Chemical Equilibrium with Applications*. Available: http://www.grc.nasa.gov/WWW/CEAWeb/

[31] M. J. Moran and H. N. Shapiro, "Fundamentals of Engineering Thermodynamics," 6th ed: John Wiley & Sons, Inc., 2008.

[32] F. W. Spaid, E. R. Keener, and F. C. L. Hui, "Experimental Results for a Hypersonic Nozzle/Afterbody Flow Field," NASA Ames Research Center1995.

[33] S. M. Ruffin, E. Venkatapathy, E. R. Keener, and N. Nagaraj, "Computational Design Aspects of a NASP Nozzle/Afterbody Experiment," presented at the 27th Aerospace Sciences Meeting, Reno, Nevada, 1989.

[34] NASA. (10/20/14). *Liquid Nitrogen Facts*. Available: http://education.gsfc.nasa.gov/dln/documents/Cryogenics%20Information.pdf

[35] T. M. Brown and N. Smith, "Reuse of a Cold War Surveillance Drone to Flight Test a NASA Rocket Based Combined Cycle Engines," presented at the Propulsion Engineering Research Center 11th Annual Symposium on Propulsion, 1999.

[36] M. Lewis. (2010) X-51 scrams into the future. *Aerospace America*. 26.

[37] J. A. Walker and J. Weil, "The x-15 program," ed, 1963.

[38] Y. Gibbs and B. Dunbar. (2014, 5 Sep. 2014). *NASA Armstrong Fact Sheet: X-15 Hypersonic Research Program*. Available: http://www.nasa.gov/centers/armstrong/news/FactSheets/FS-052-DFRC.html#.VGgG1PnF_1A

[39] "MIL-DTL-87107E Propellant, High Density Synthetic Hydrocarbon Type, Grade JP-10," ed: United States Department of Defense, 2012.